Spring 5-31-2003

Optimization for source localization and geoacoustic inversion in underwater acoustics

Urmi Ghosh-Dastidar
New Jersey Institute of Technology

ABSTRACT

OPTIMIZATION FOR SOURCE LOCALIZATION AND GEOACOUSTIC INVERSION IN UNDERWATER ACOUSTICS

by
Urmi Ghosh-Dastidar

Matched-field inversion techniques are widely used for source localization and geoacoustic parameter estimation. These inversion methods correlate the received data with modeled data and find the model parameters which provide the maximum correlation. However, when a large number of unknown parameters is involved, many modeled data need to be generated and correlated with the observed data and thus, matched-field inversion can be computationally intensive. An optimization process applied to matched-field inversion is often required to accelerate the inversion process.

In this work, *tabu* is applied to matched-field inversion for source localization and environmental parameter estimation. Tabu is a global optimization technique which proceeds by finding the best model in a local neighborhood, where a best model is defined as the set of parameter values that provides the maximum correlation in a given neighborhood. However, the search moves beyond local areas by maintaining records of past moves. Using historical information, the approach avoids certain paths. Thus, tabu limits the search space and redefines neighborhoods in each iteration. Tabu is evaluated through a comparison to fast simulated annealing.

To improve efficiency, a tabu approach is also developed for parameter estimation in a rotated coordinate system. Rotation is achieved through the identification of combinations of parameters that affect acoustic field computations.

OPTIMIZATION FOR SOURCE LOCALIZATION AND GEOACOUSTIC INVERSION IN UNDERWATER ACOUSTICS

by
Urmi Ghosh-Dastidar

A Dissertation
Submitted to the Faculty of
New Jersey Institute of Technology and
Rutgers, The State University of New Jersey – Newark
in Partial Fulfillment of the Requirements for the Degree of
Doctor of Philosophy in Mathematical Sciences

Department of Mathematical Sciences
Department of Mathematics and Computer Science, Rutgers-Newark

May 2003

APPROVAL PAGE

OPTIMIZATION FOR SOURCE LOCALIZATION AND GEOACOUSTIC INVERSION IN UNDERWATER ACOUSTICS

Urmi Ghosh-Dastidar

5/6/03

Dr. Zoi-Heleni Michalopoulou, Dissertation Advisor — Date
Associate Professor of Mathematical Sciences Department, NJIT

5.6.03

Dr. Daljit S. Ahluwalia , Committee Member — Date
Chair of Mathematical Sciences Department, NJIT

5/6/03

Dr. Jonathan H. C. Luke , Committee Member — Date
Professor of Mathematical Sciences Department, NJIT

5/6/03

Dr. John K. Bechtold, Committee Member — Date
Associate Professor of Mathematical Sciences Department, NJIT

5/6/03

Dr. Richard Haddad, Committee Member — Date
Professor of Electrical and Computer Engineering, NJIT

BIOGRAPHICAL SKETCH

Author: Urmi Ghosh-Dastidar

Degree: Doctor of Philosophy

Date: May 2003

Date of Birth:

Place of Birth:

Undergraduate and Graduate Education:

- Doctor of Philosophy in Mathematical Sciences,
  New Jersey Institute of Technology, Newark, NJ, 2003
- Master of Science in Applied Mathematics,
  New Jersey Institute of Technology, Newark, NJ, 1998
- Bachelor of Science in Applied Mathematics,
  Ohio State University, Columbus, OH, 1996

Major: Applied Mathematics

Presentations and Publications:

Z. -H. Michalopoulou, U. Ghosh-Dastidar,
"Tabu optimization for matched-field inversion,"
The Journal of the Acoustical Society of America, 112, November, 2002.

Z. -H. Michalopoulou, U. Ghosh-Dastidar,
"Tabu for source localization and geoacoustic inversion,"
The First International Conference. Inverse Problems: Modeling and Simulation,
Fethiye, Turkey, July, 2002.

U. Ghosh-Dastidar, Z. -H. Michalopoulou,
"New approaches for detection and source localization,"
Oceans 2001 Conference, Honolulu, Hawaii, November 2001.

Z. -H. Michalopoulou, X. Ma, M. Picarelli, U. Ghosh-Dastidar,
"Fast matching methods for inversion with underwater sound,"
Proceedings of Oceans 2000 MTS/IEEE Conference, Providence, Rhode Island,
September 2000.

U. Ghosh-Dastidar, Z. -H. Michalopoulou,
"Inverse problems in underwater acoustics in the presence of internal waves,"
AWM Workshop at SIAM Annual Meeting, Rio Grande, Puerto Rico, July 2000.

To my dearest parents, Mr. Bimalendu Dutta Gupta and Mrs. Utsa Dutta Gupta,
without whom this would not have been possible

ACKNOWLEDGMENT

This work would not have been possible without the advice and cooperation of my advisor Dr. Zoi-Heleni Michalopoulou. In these past few years, she was always there to provide me with proper guidance including valuable insights in a host of technical matters. I sincerely express my deepest gratitude to her.

I would like to acknowledge Dr. Daljit S. Ahluwalia for his continuous assistance and many words of encouragement and motivation over the years. My heartfelt thanks go to him for his untiring support and also serving as my dissertation committee member.

I would also like to thank Dr. Jonathan H. C. Luke, Dr. John K. Bechtold, and Dr. Richard Haddad for serving as my dissertation committee members. It is their help and cooperation that finally makes this work successful.

My thanks must also go to all faculty members, Ms. Padma Gulati and Ms. Susan Sutton. I consider myself privileged for having the opportunity to work with all of them.

I would also like to thank Knograt Savettaseranee (Kelly) and Said Kas-Danouche for their immense support in some of the most difficult times. Special thanks go to Kelly who was always there for me during all these years.

My thanks also go to Hoa K. Tran, Lyudmyla Barannyk, Jyoti Champanerkar, Lin Zhou, Arnaud Goullet and Sanjeev Bokhoree for their friendship and help.

I also would like to thank Dr. Swati Neogi for providing me endless encouragement and advice during all these years.

My thanks must also go to my sister-in-law, Sucharita Das and brother-in-law, Priyaranjan Das for taking care of my son while I was busy with finishing up my dissertation. Special thanks to my sister and brother-in-law, Nandini Sen Gupta and Dr. Tapas Sen Gupta, for their unfaltering support which helped me keep going.

At the end, I would like to thank my parents for their infinite love and affection. They were a great source of support and motivation for me through out all these years. I feel very grateful to my brother, Samudra Dutta Gupta who was there for me in every step of the way giving support and inspiration. His encouraging words helped me through some of the very challenging periods in my life. I also like to thank my sister-in-law, Mousumi Dutta Gupta for taking care of my parents while I am thousands of miles away from them; without whose assurance I cannot achieve this. I am also grateful to my uncle and aunt, Mr. Parimalendu Dutta Gupta and Ms. Manju Dutta Gupta for their unending love towards me. In addition, I like to thank my aunts and uncle, Mrs. Anupama Sen, Mrs. Supti Dutta Gupta, and Mr. Nirmalendu Dutta Gupta for providing me inspiration throughout my Ph.D. student life.

Last, but not least, I thank my husband Dr. Abhijit Ghosh-Dastidar for his understanding and love. Without him, I can never be the person, who I am now. His support, encouragement, and cooperation provided stimulant for sailing through this period.

TABLE OF CONTENTS

TABLE OF CONTENTS
(Continued)

Chapter **Page**

LIST OF TABLES

Table **Page**

LIST OF TABLES
(Continued)

Table **Page**

LIST OF FIGURES

LIST OF FIGURES
(Continued)

Figure **Page**

CHAPTER 1

INTRODUCTION

An **inversion scheme** is a process which predicts values of unknown parameters using a decision rule together with a search algorithm, given a set of observed data. Inversion plays a significant role in underwater signal processing for source localization of acoustic sources and estimation of geoacoustic parameters such as bottom depth, sediment thickness, attenuation, and bottom sound speed among others.

Matched field processing (MFP) [1, 2, 3, 4, 5, 6] is widely used as an inversion technique for source localization and environmental parameter estimation in the ocean. This scheme solves the Helmholtz equation (**forward modeling**) by using different values for the unknown parameters repeatedly and generates many **replicas (solutions of the Helmholtz equation)** at the receiving hydrophones. MFP then correlates replicas to the received data and determines the parameter values which maximize the data-replica correlation.

A grid-based exhaustive search applied to MFP provides the most accurate estimates. However, when several parameters are unknown, many replicas must be generated and matched to the observed data, making an exhaustive search computationally inefficient. An optimization method together with MFP is needed to accelerate the search in the parameter space, by exploring more heavily probable solutions rather than the whole space.

There exist several optimization approaches. Simulated annealing (SA) [7, 8, 9, 10] and genetic algorithms (GA) [11] are the most widely used global optimization processes for localization and geoacoustic inversion. The SA approach is a Monte Carlo process which randomly perturbs the current model, where a model is defined as a multi-dimensional vector, consisting of possible values of the unknown parameters. The process accepts all models which improve the optimizing function; some downhill

steps which lower the objective function value are also accepted probabilistically. SA ensures convergence to the global maximum if the temperature schedule, the initial temperature, and the parameter perturbations are appropriate. However, this approach takes a substantial amount of time to converge and, also, the appropriate annealing schedule is, in practice, found by trial and error. The fast SA [12] method, where the cooling rate is inversely proportional to the iteration number, provides faster convergence than the traditional SA method. However, again, the performance of the process depends strongly on the temperature schedule and other factors that can be determined only empirically. Gerstoft uses GA for localization and geoacoustic parameter estimation [11]. The GA technique is based on simulating the evolution of population models based on a set of stochastic criteria. This process imitates genetic crossover and mutation (random perturbations) in favor of higher correlation. Although this approach often identifies a wide area around the global maximum, the method does not always perform well locally [13]. Gibbs sampling [14] is another global optimization process which involves the estimation of multi-dimensional integrals of the posterior probability density of the unknown model parameters, typically performed by using a sampling procedure. However, this process is also computationally intensive when several unknown parameters are involved; its performance also depends on the validity of prior assumptions. Chapman and Lindsay [15, 16] developed a scheme which they refer to as "adaptive simulated annealing," which does not need a predetermined temperature schedule like traditional SA. Instead, the temperature is related to the sensitivity of the acoustic field to each parameter during the inversion. This method uses matched field correlation information to guide the search adaptively towards models which are associated with high values of the optimizing function. Thus, this method has the ability to learn and guide the search during inversion. Unlike SA, where one searches for one final highest correlation value, Jaschke and Chapman [17, 18] developed a freeze bath approach which generates a set of different

models all of which match the data well. The main difference of the method with conventional SA is the usage of temperature. The freeze bath method involves sampling new models at a fixed temperature during the search, whereas SA involves decreasing the temperature stepwise. Fallat and Dosso [19] developed a simplex simulated annealing (SSA) approach which takes advantage of the local downhill simplex method, where downhill corresponds to moving down into a valley in the optimizing function space when one searches for the global minimum. Since we are interested in maximization, instead of moving downhill, the search needs to move uphill in the optimizing function space. Although SSA uses the local downhill simplex method, the search can escape a local minimum (maximum in our case) by accepting uphill steps based on a stochastic component.

Tabu [20, 21, 22, 23] is a relatively novel optimization process which, to the best of our knowledge, has not been used in underwater acoustic signal processing. While most other existing optimization methods rely on stochastic criteria, the key feature of tabu is to de-emphasize randomness and rely, instead, on memory. In tabu, a *move* is defined as a parameter change from a set of old parameter values to a set of new parameter values. The method uses several prohibition lists based on different criteria; the process updates the lists in every iteration and forbids moves which are contained in the prohibition lists. In every iteration, the search creates a local neighborhood, scrutinizes each model in that neighborhood by inspecting the lists, and proceeds to search the parameter space by accepting the best possible move. Since, in each iteration, tabu redefines the neighborhood, this method is also referred to as a *variable neighborhood method* [20]. The current work is different from previous work on tabu in the following way. Here, we introduce three different lists based on three different criteria: the first list is generated to prohibit exploration of unlikely solutions by forbidding a move from a better solution to a worse solution, the second list is used to avoid cycling, and the third list is introduced to improve efficiency.

While searching the parameter space, if all the moves in the current iteration are forbidden, the current neighborhood becomes empty and the search gets trapped. Therefore, an escape mechanism based on the first two lists mentioned above is also defined for better exploration of the search space. This new mechanism, which is introduced here, helps tabu to escape from such "traps".

First, we apply tabu for inversion in a conventional coordinate system. Next, we reparametrize the parameter space and implement tabu in a rotated coordinate system. If the most prominent hill in the optimizing function space (associated with the global maximum) is obliquely oriented to the original coordinate axes, navigation could be inefficient if the search is performed by using the regular coordinate system. Instead, if the coordinates are rotated so that the new axes become parallel and perpendicular to the most significant hills of the optimizing function space, efficiency can be attained. Lately, a coordinate rotation in searches has attracted a lot of attention [24, 25, 17, 18]. We implement such a rotation by finding mutually orthogonal eigenvectors of the covariance matrix of the gradient of the optimizing function.

Tabu is also applied to inversion with real data. Specifically, source location and environmental parameters are estimated using the SWellEX-96 experimental data.

The work presented in this dissertation is structured as follows: the basic elements of MFP are described in Chapter 2. Tabu, as developed here, is presented in Chapter 3. Tabu is evaluated on parameter estimation through a comparison to fast SA in Chapter 4. The principles and mechanics of coordinate rotation are discussed in Chapter 5; tabu is, then, implemented in rotated coordinates and compared to regular tabu. In the same chapter, the performance evaluation includes SA in regular and rotated coordinates. A comparison is, then, performed between tabu in rotated coordinates and SA in the same coordinates. Real data inversion is also performed, and the corresponding results are discussed in Chapter 6. Finally, the work is summarized in Chapter 7.

CHAPTER 2

MATCHED FIELD PROCESSING, NORMAL MODE METHOD

In the process of localization and geoacoustic parameter estimation in underwater acoustics, three issues need to be addressed: the selection of a suitable **forward model** for calculating **replica fields**, the selection of a **decision criterion**, and the design of an **optimization procedure** for efficient inversion.

2.1 The Forward Model Component: Modeling Sound Propagation with Normal Modes

There exist several numerical forward modeling schemes for sound propagation based on ray theory, normal mode theory (NM), the fast field program (FFP), the parabolic equation (PE), and the finite difference method among others [26, 6]. Ray theory involves obtaining a high-frequency asymptotic solution of the Helmholtz equation. Thus, this method is more suitable for high frequency sound propagation modeling. The fast field program (also referred to as the wavenumber integration technique) obtains an integral transform solution of the Helmholtz equation in a horizontally stratified medium. Although this method provides almost exact solutions for all frequencies, the method is computationally expensive. Starting with the Helmholtz equation and then using an asymptotic Hankel function in its solution, the PE method obtains a parabolic wave equation. This method is mostly used for inversion in range dependent propagation problems. The finite difference method uses a direct discretization technique to solve the wave propagation equation. This method is difficult to implement computationally, but is particularly useful when boundary scattering effects need to be considered in the sound propagation model.

We have used the NM approach for our work [27, 28, 26]. This approach provides fast results for low frequencies since few modal calculations are needed in such cases, making the method computationally attractive. Moreover, this method is suitable

for long range propagation. Since we have chosen to work with low frequency and relatively long range, the NM method is appropriate for our environment. The NM model is briefly presented below [26].

For a point source in a two-dimensional space in frequency domain, the Helmholtz equation can be written as:

$$\frac{1}{x}\frac{\partial}{\partial x}(x\frac{\partial p}{\partial x}) + \rho(z)\frac{\partial}{\partial z}(\frac{1}{\rho(z)}\frac{\partial p}{\partial z}) + \frac{\omega^2}{C^2(z)}p(x,z) = -\frac{\delta(x)\delta(z-z_s)}{2\pi x} \tag{2.1}$$

where the range x is the distance between the source and the receiver, z_s is the source depth, ρ is the density, p is the pressure of the water particle, $C(z)$ is sound speed, and ω is the angular frequency.

Let $p(x,z_s) = \phi(x)\chi(z_s)$. Using separation of variables we obtain the modal equation. Finally, assuming a pressure release surface and a perfectly rigid bottom, and using an asymptotic approximation we arrive at the following solution [26]:

$$p(x,z_s) = \frac{i}{4\rho(z)}\sum_{m=1}^{M}\chi_m(z_s)\chi_m(z)\frac{\exp(ik_m x)}{\sqrt{k_m x}} \tag{2.2}$$

where k_m is the eigenvalue of the modal equation, $\chi(z_s)$ is the eigenfunction, and M is the number of propagating modes. This solution is derived for range independent environments. However, the normal mode method can be easily extended to range dependent cases using the adiabatic approximation [26].

2.2 Matched Field Processing for Inversion

Matched field processing correlates the data vector **d** with the replica vector **r**, where each element of **r** is the solution p obtained by solving the Helmholtz equation for each receiving hydrophone. MFP then finds values of the unknown parameters that maximize the correlation.

To summarize, the whole process can be described as follows:

1. Collect **d** (data) at receiving hydrophones.

2. Decide N, the number of parameters to be estimated.

3. Decide $\mathbf{D_N}$, the search domain for the N parameters.

4. Select models **m** from $\mathbf{D_N}$ by using a search process, where a model is a vector of values for the unknown parameters.

4a. Create many replica vectors **r** (as mentioned above, each element of the replica vector corresponds to the solution p in Equation 2.2) by calculating the field for the parameter values of **m**.

4b. Match replica vectors **r** to the observed data **d** by using a correlation criterion.

5. The estimates of the unknown parameters are those which are associated with the best match between replicas and data.

There are several processors that match data and replicas for matched field inversion. The minimum variance processor [6] is very sensitive to modeling errors. Thus, a very accurate and detailed environmental knowledge is necessary. The optimum uncertain field processor [29] is based on modeling an unknown or inaccurately modeled environment. This processor requires a multi-dimensional integration over all unknown environmental parameters, which is computationally expensive. The

Bartlett processor [6] is well known for its simplicity and insensitivity to environmental mismatch. This processor calculates an inner product between observed and replica fields in the frequency domain. For its simplicity and robustness, we have chosen the Bartlett processor for MFP. This processor computes correlation or ambiguity function F, where:

$$F = \left| \frac{\mathbf{d}^\dagger}{\|\mathbf{d}\|} \frac{\mathbf{r}}{\|\mathbf{r}\|} \right|^2 \tag{2.3}$$

where $\mathbf{r}$ is the replica vector and $\mathbf{d}$ is the received acoustic field. Symbol $\dagger$ means conjugate transpose.

The estimates of the unknown parameters are those which are associated with the maximum value of F.

CHAPTER 3

TABU

3.1 Tabu: Background

Tabu is a global optimization method which makes extensive use of memory [20, 21, 22, 23]. The search creates a local neighborhood in each iteration and selects the best model from this neighborhood, where the best model is associated with the maximum correlation found in the given neighborhood. In the next iteration, tabu starts searching from the neighborhood of the model selected in the current iteration. However, selection of new models is subject to restrictions. These restrictions are placed by tabu through the creation of lists. In every iteration, the process updates the lists with new information obtained from the current selection of the best model and discards the oldest information from the lists. If a move between models is contained in a list, then the move has tabu status, which means that the move cannot be accepted. In this situation, tabu rejects the move, reduces the size of the local neighborhood by eliminating the model associated with this move, and proceeds by searching for the best model in the reduced neighborhood. If a move is not contained in the lists, then this move is acceptable.

Glover has done extensive work on tabu search and provides many examples to illustrate how tabu searches the space intelligently by learning from the past history [20]. Numerous examples of discrete optimization problems are provided and different tabu strategies in these contexts are discussed [20]. Vinther and Mosegaard implement tabu search in seismic inversion [22]. They suggest the use of a non-random strategy to solve these highly nonlinear problems. According to them, tabu, as they implemented it, is primarily a natural process, similar to the way one might use to solve a problem manually by using common sense. At each iteration of this inversion process, the method generates a new neighborhood, selects the best model from the non-tabu

neighbors, and remembers the reverse of the current parameter change. The search also stores the solution obtained by the best model, found in the previous iteration. From now on, if a parameter change from the old model to a model in the current neighborhood is enlisted and the old model has higher solution quality than the current one, then the parameter change from the old model to this current model cannot be accepted. Dervis and Duc also provide an extensive discussion on tabu [23]. In their work, an adaptive mechanism is used to produce neighbors in each iteration. The neighbors are generated based on a criterion which uses the information of the iteration number when the latest improvement is obtained. They develop two different tabu restrictions which are built on recency and frequency memory conditions. Failure to satisfy either one of these two restrictions by an element of a model imposes tabu status on this element. In each iteration, the performances of non-tabu neighbors are estimated and the search selects the neighbor which provides the highest improvement from the current solution. However, if none of these neighbors is able to produce an improvement, then the performance of the i-th neighbor is again estimated by using a criterion based on improvement, recency, and frequency. This time, the improvement is a measure equal to the difference between the performance of the current solution and that of the i-th neighbor. The existing work on tabu essentially describes that use of memory is a key factor for efficient searches.

We may say that Chapman and Lindsay first introduced a global search method in underwater inversion similar to tabu [15, 16]. For each field replica, the received data and the replica field are correlated. The models which produce higher correlations are accepted unconditionally; the models with lower correlations are accepted conditionally with a Boltzman probability distribution similarly to SA. However, this process does not use a predetermined annealing schedule like traditional SA. Instead, this adaptive technique uses correlation information in each iteration and guides the search towards models which have above average correlation. Thus, in a sense, as tabu does,

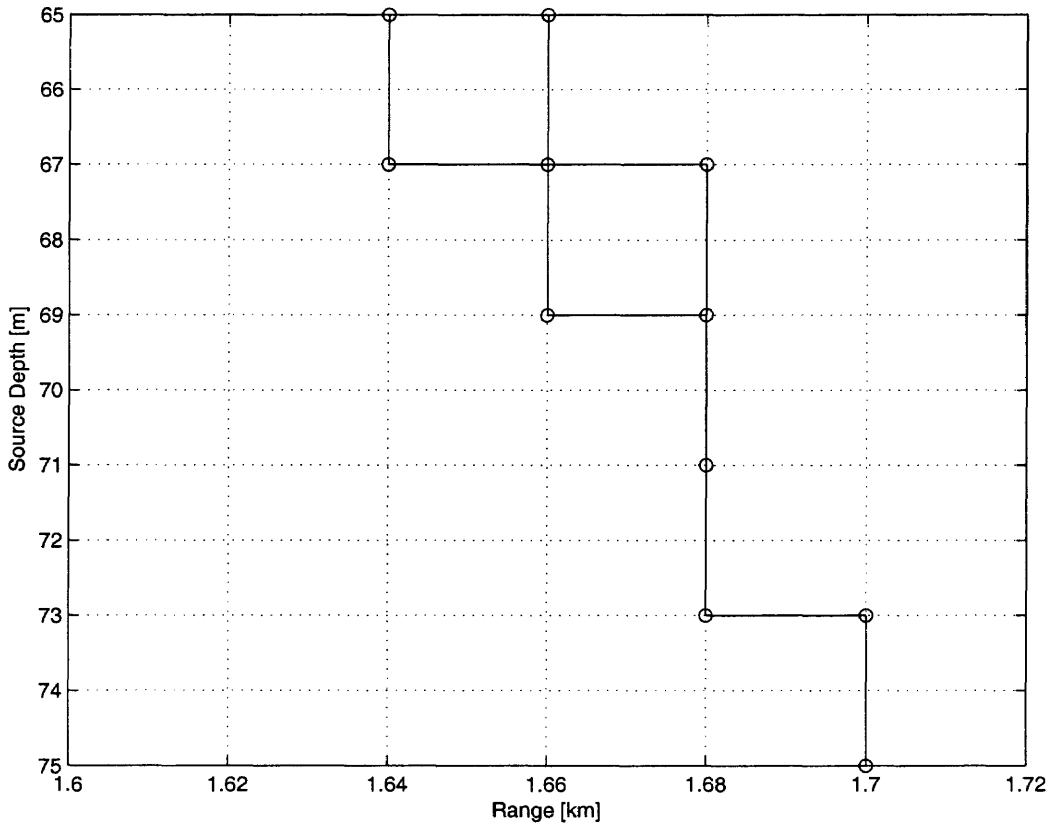

Figure 3.1 Cycling occurs for 2-D inversion.

this procedure learns and acts while searching the parameter space and restricts the search space to save computational time by discouraging exploration of unlikely solutions.

3.1.1 Tabu Lists

Lists are essential elements of tabu. One of the primary roles of the lists is to prohibit cycling: cycling is the repeated visitation of the same local neighborhood or repetition of the same search path. This situation could arise if a search accepts a model which was recently visited and follows the same search pattern thereafter. By using historical information from the lists, tabu attempts to avoid cycling by discouraging visitation of recently explored models. However, cycling could still occur, even under the restrictions of tabu lists. Figure 3.1 shows an example of cycling. The process

employed to illustrate cycling in Figure 3.1 uses a list according to which the changes of parameter values which are accepted cannot be reversed for a certain number of iterations. Therefore, if tabu moves from a model m_c to a model m_d, the process is not allowed to move in the reverse direction, that is, from m_d to m_c. In Figure 3.1, tabu starts searching from 1.7 km of range and 75 m of the source depth. Each circle in this figure represents the best model found by tabu in every iteration. Although from this figure one might think that the process stops when the search reaches either one of the points (1.64,65) or (1.66,65), actually the search never stops. Tabu follows the same search path and keeps repeating it. Therefore, if the list type is not appropriate, cycling could occur. List size is also important for the prevention of cycling. The appropriate size depends on the dimensionality of the problem and is usually found empirically.

3.2 Tabu Search in Underwater Acoustic Signal Processing

Implementing a prohibition policy by using memory, we build a tabu approach suitable for matched-field inversion. In each iteration, the neighborhood size is chosen to be $2(unk - par)$, where $unk - par$ is the number of unknown parameters. This neighborhood is chosen so that each parameter is perturbed in both positive and negative directions in each iteration. The parameter perturbations are fixed. Therefore, in a two-dimensional search, a neighborhood contains all four center points of the sides of a square, in a three-dimensional search a neighborhood contains all six center points of the sides of a cube and so on. In summary,

$$\hat{x}_i = x_i \pm \Delta x_i \tag{3.1}$$

where $\hat{x}_i$ is the i-th perturbed parameter value, x_i is the current value of the i-th parameter, and Δx_i is the fixed perturbation for the i-th parameter.

Lists: We use two different tabu lists, based on two different criteria:

List 1: While performing inversion with tabu, we notice that there are situations when none of the neighboring models in the current neighborhood offers better solution (higher correlation) than the previously accepted model. In such cases, if tabu accepts the best model (from the neighborhood) which has a lower correlation than that of the previously found best model, there could be situations when tabu proceeds downhill for several iterations. This behavior sometimes forbids tabu to explore models associated with high correlation. To avoid that, a list that maintains a history of recent improvements is introduced; the list is referred to as the reverse improvement list. If the best model found in the current neighborhood provides a better solution than the previous model, the change of parameter values from the old model to the current one leads to an improvement. In such a case, the reverse of the change (reverse of the improvement) is stored in the reverse improvement list. Since all moves contained in the reverse improvement list provide worse solutions, accepting these moves leads the process to lower correlation regions. For this reason, the moves contained in this list are prohibited and all of these moves are considered tabu. For the reverse improvement list, we need to have a list size of at least $2(unk - par)$. Since in each iteration, tabu creates a neighborhood of size $2(unk - par)$, there are $4(unk-par)$ number of forward and reverse moves associated with each neighborhood; having a list size smaller than $2(unk - par)$ might allow tabu to accept a model (whose neighborhood has already been explored) with worse correlation than that of the current model.

List 2: If unrestricted, tabu might sometimes repeat a search path by accepting forward moves which have been previously explored. To avoid repetition, a second list, referred to, here, as the forward list, is introduced; the forward list contains all

recent forward moves. The moves contained in this list cannot be repeated for several iterations to prevent repeated occurrence of the same search pattern. A list size of l enables the process to avoid cycling for l iterations. However, there are no rules for accurately choosing the optimal list size. The size has to be chosen by trial and error.

Jump Condition: If a move is contained in either one of the lists mentioned above, then this move is prohibited. When all moves are prohibited by tabu lists, tabu cannot proceed further and the process gets trapped. In Figure 3.2, an example of trapping is shown. Here, we have used the two lists which were mentioned above. The search starts from 1.7 km of range and 75 m of source depth. The search reaches a local maximum at 1.66 km of range and 67 m of source depth. By using information from the reverse improvement list, tabu learns that all neighborhood points have lower correlation than the local maximum. Thus, tabu cannot move back from the maximum to any neighbors, since that would mean reversal of improvements. Unless forced to continue, the process will then stop.

To avoid such an occurrence, we introduce the concept of a random step jump. When moves to all neighbors are prohibited, the search generates a random integer k which provides modified step sizes for the current iteration. For exploring the search space better, a bigger neighborhood size is chosen by using three different steps $(k, 2k, 3k)$. Tabu, then, creates neighborhoods using these step sizes, selects the best model in these neighborhoods, and jumps out of the local neighborhood by starting a new search from the best model found. The perturbations in case of a jump are performed diagonally by perturbing all parameters at a time as follows:

$$\hat{x}_i = x_i \pm k_j \Delta x_i \tag{3.2}$$

where j=1,2,3, $k_1 = k$, $k_2 = 2k$ and $k_3 = 3k$, $\hat{x}_i$ is the i-th perturbed parameter value, x_i is the old value of the i-th parameter, and Δx_i is the i-th parameter perturbation. In a diagonal perturbation, a neighborhood contains four vertices of a square in

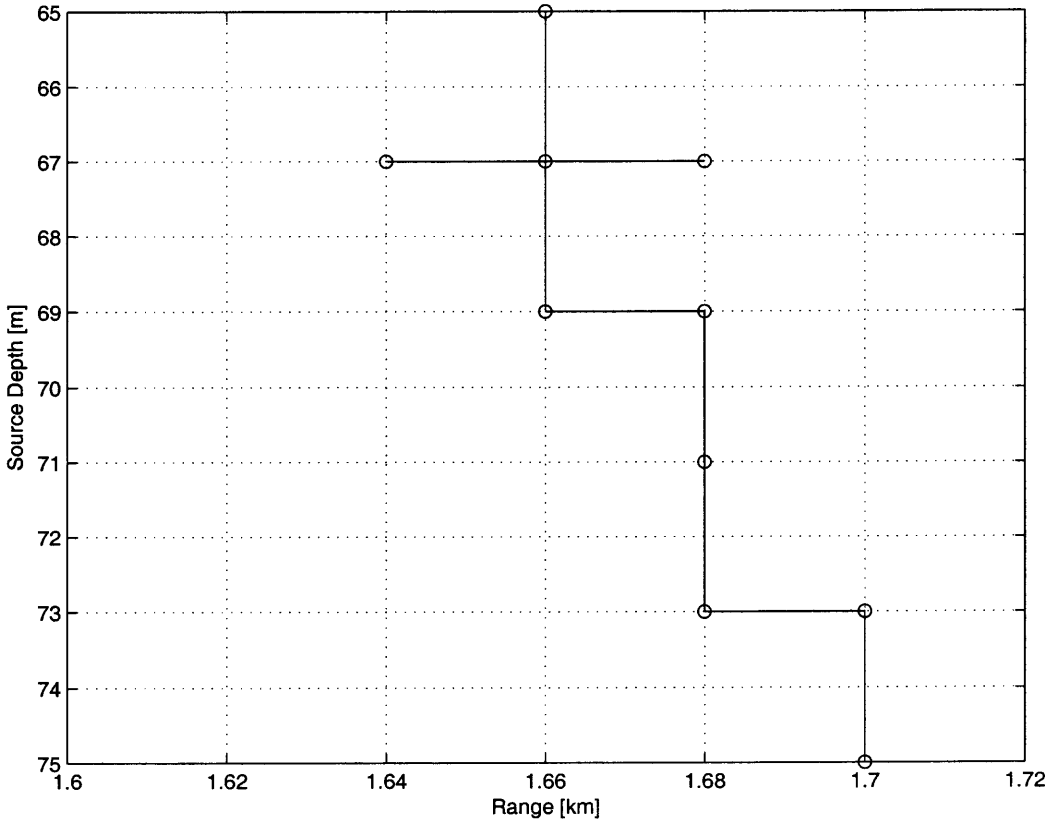

Figure 3.2 Trapping occurs for 2-D inversion.

two-dimensional inversion, eight vertices of a cube in three-dimensional inversion and so on. In other words, for an n-dimensional inversion, we require 2^n neighbors. This diagonal perturbation is performed for diversification of the search process.

Once the search moves out of the trap to the new model, parameter perturbations follow again Equation 3.1. As an illustration of the trapping and the subsequent random jump of tabu, the following example is provided. An acoustic source of 150 Hz is placed at 2 km of range and 100 m in depth in a 216.5 m deep ocean. The signal is received in a noise-free environment at an array of ten vertically separated hydrophones between 50 m and 140 m. Two-dimensional inversion is performed by assuming that source range and source depth are unknown. The true values of the unknown parameters and the bounds on various parameters are given in Table 3.1.

Table 3.1 The True Values of the Parameters and the Bounds on Parameters : x_s = Range, z_s = Source Depth

No	Parameters	True	Minimum	Maximum
1	x_s - km	2.0	0.01	5.0
2	$z_s - m$	100.0	0.0	200.0

Figure 3.3 shows the complete search starting with an initial model (3.2, 152) corresponding to source range and source depth. As a comparison, exhaustive search results (the ambiguity surface discussed in Chapter 2) are superimposed in the same figure.

The red regions correspond to high optimizing function values, the yellow regions have lower optimizing function values than the red regions, and the blue regions correspond to the lowest optimizing function values. This figure demonstrates the search pattern that tabu follows. When trapped in the vicinity of the initial model, tabu generates random steps. The search then explores all neighborhood models created by these random steps and chooses the best model. A new search then

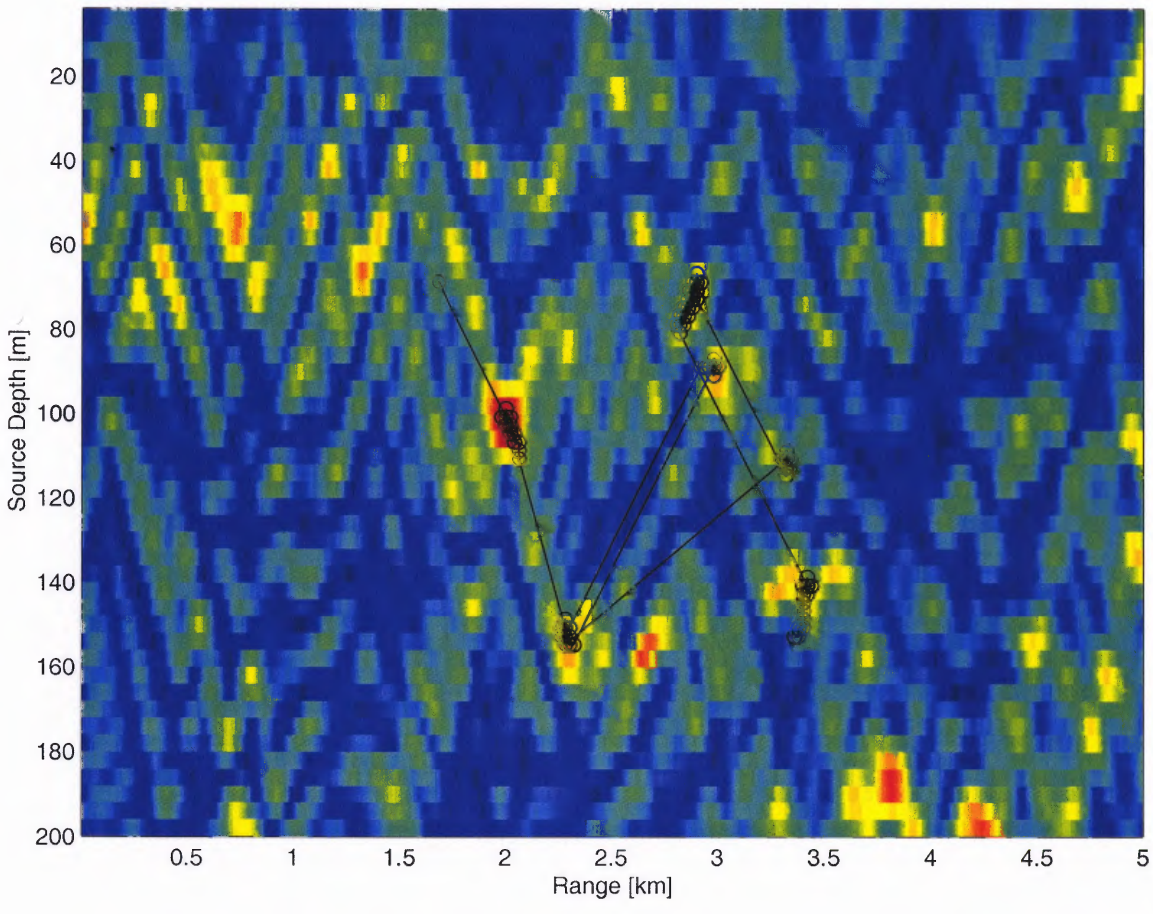

Figure 3.3 An example of a 2-D tabu search superimposed on the Bartlett ambiguity surface.

starts from the neighborhood of the chosen model. We observe that, as tabu jumps, it chooses a model associated with a local maximum and, thus, is more likely to explore high correlation regions more frequently than low correlation regions. Due to randomness in the jumps, the chance of visiting the same neighborhood repeatedly is remote. In Figure 3.3, we also notice that, while tabu jumps from the vicinity of the initial model to (2.6,76), the search does not revisit the starting model. Instead, the search subsequently jumps to (3.4,116).

Tabu has been so far discussed for two-dimensional inversion for demonstration purposes. In practice, in a more realistic environment, the receiver location parameters as well as environmental parameters could be unknown as well. Thus, we extend the search to nine-dimensional inversion by assuming that the ocean depth, sediment thickness, bottom sound speeds, attenuation, receiver shifts, and tilt are unknown. For higher dimensional inversion, the neighborhood size for jumps needs to be carefully selected. As we increase dimensionality, forming diagonal neighborhoods demands more forward model calculations, since $2^{unk-par}$ becomes large as we increase the number of unknown parameters. Therefore, we have chosen this size as $3(2^4)$. The reason for this selection is as follows. Figure 3.4 demonstrates the sensitivity of the optimizing function with respect to nine parameters. The sensitivity of the optimizing function to a particular parameter is defined as the pattern of change of the optimizing function with respect to changes in that parameter. Usually, a small change in a source location parameter affects the optimizing function more than a change in other parameters [24]. For this reason, while jumping, the neighborhood is generated based on the number of important parameters, where important parameters are the parameters that affect the optimizing function the most. By inspecting Figure 3.4, we notice that the optimizing function is affected more prominently by source range and depth. Within the given boundaries of these two parameters, the optimizing function varies from approximately 0 to 1. The sensitivities of the optimizing function to tilt

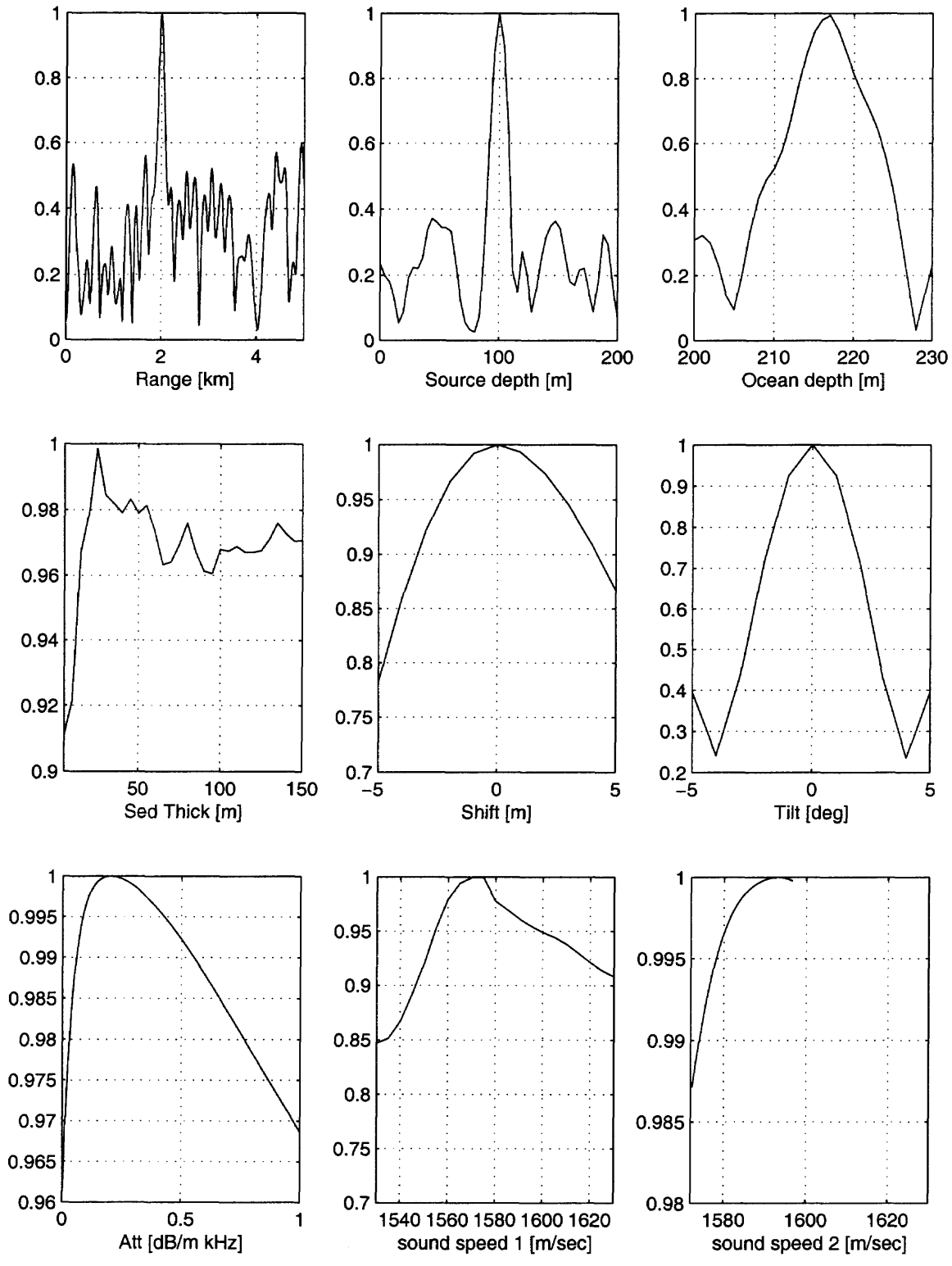

Figure 3.4 Sensitivity of optimizing function to different parameters.

and ocean depth are almost identical and follow the function sensitivity to range and source depth. The other examined parameters affect the function less than the above mentioned four parameters. Since the optimizing function is not expected to change significantly if any of these remaining five parameters are changed, we only perturb range, source depth, tilt, and ocean depth when jumping, to avoid unnecessary forward model calculations.

List 3: Besides having the reverse improvement and the forward lists, we also create a third list, which we refer to as the neighborhood list. This list contains all models and the respective values of the optimizing functions which have been recently explored by tabu. Tabu does not have to recalculate the optimizing function if a model is contained in the third list, since the value of the optimizing function is already listed. Since most of the search time is spent on calculating the forward models, having the third list is beneficial to speed up the inversion process. There is no optimum criterion for this list size selection. This list is particularly helpful when a broadband propagation problem is considered. In a broadband inversion problem, to calculate the optimizing function for a specific model, the forward problem needs to be solved for each involved frequency. If a particular model has already been visited and the corresponding value of the optimizing function is enlisted, then numerous forward model calculations do not have to be repeated.

In each iteration, tabu updates each list and discards old moves (from the reverse improvement or the forward lists) and old models (from the neighborhood list). The search stops when the number of forward models exceeds a specified value. A flowchart of tabu is shown in Figure 3.5.

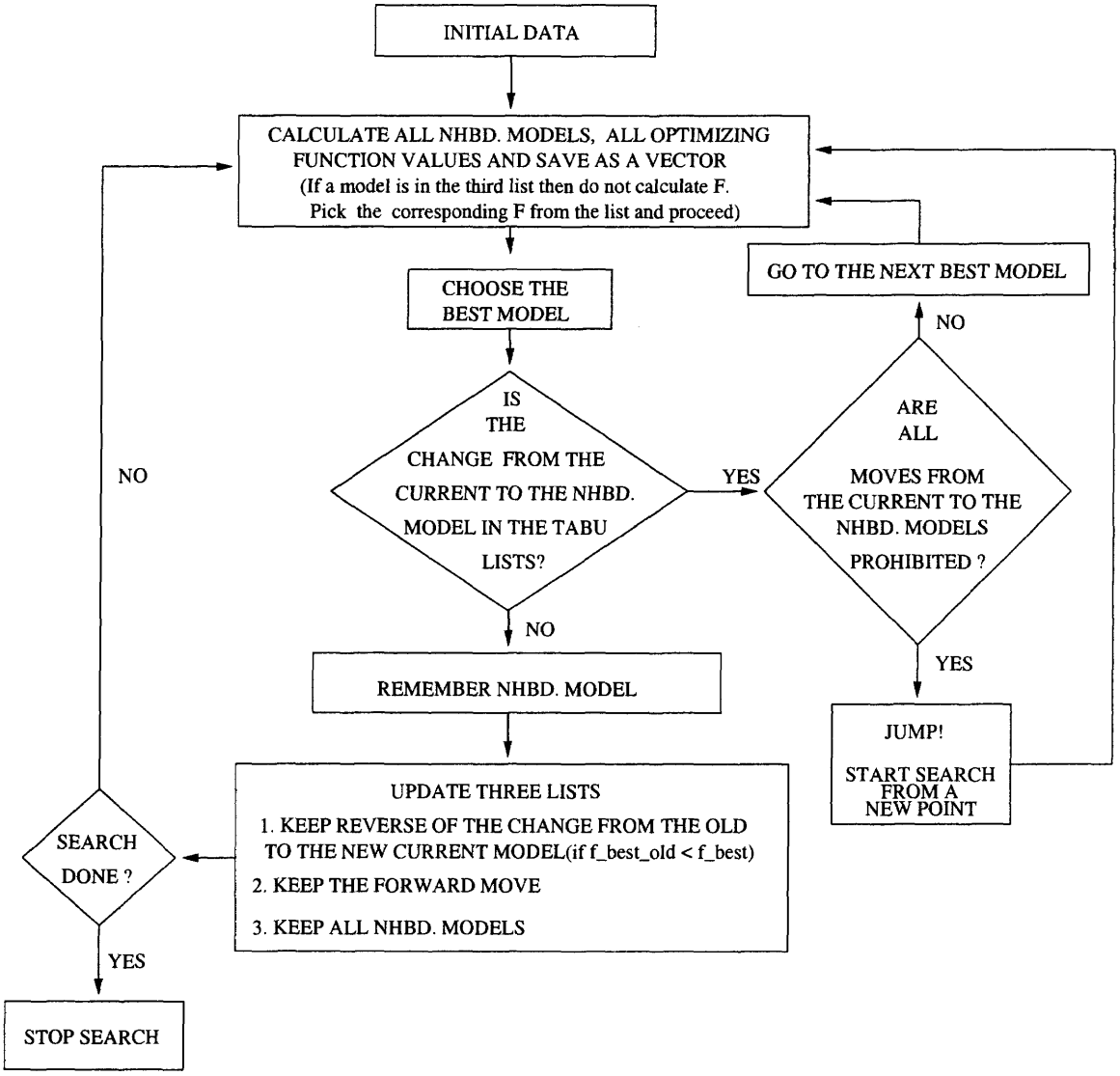

Figure 3.5 Tabu flowchart.

CHAPTER 4

COMPARISON BETWEEN TABU AND SA

In this chapter, we present results obtained by tabu and SA with synthetic data. The environment used to generate the data simulates the SWellEX-96 experiment, performed in California in the Summer of 1996. The environment is shown in Figure 4.1. The water column is 216.5 m deep followed by a relatively thin sediment layer. A vertical array of ten receiving hydrophones is located at 2 km away from the source. The hydrophones have a 10 m vertical spacing, the shallowest hydrophone being at 50 m in depth.

Before the comparison, as a test, we perform a two-dimensional tabu search for source localization (assuming that the source range and depth are unknown). This search is performed for ten different initial conditions. The true values are presented in Table 3.1. The results are shown in Table 4.1. From column two to four of the table, the estimates of the source range and depth and the corresponding maxima found by tabu for each initial condition are shown, whereas the fifth column provides the required number of objective function calculations by tabu to obtain the global maximum. We observe that tabu locates the source accurately in an efficient manner.

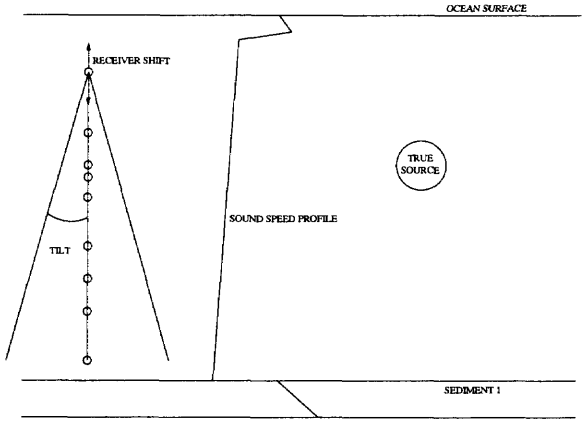

Figure 4.1 Sound speed profile for simulation.

Table 4.1 Tabu Results: 2-D; R = Range, S D = Source Depth, O D = Ocean Depth, max = Maximum Found, Models = Number of Forward Models Needed to be Calculated to Reach the Global Maximum

Initial Data	R	S D	max	Models
1	1.99	99.93	0.99	79
2	2.00	99.91	0.99	659
3	1.99	99.85	0.99	681
4	2.00	100.43	0.99	291
5	1.99	99.26	0.99	230
6	1.99	100.93	0.99	352
7	1.99	100.82	0.99	1439
8	2.00	100.75	0.99	225
9	1.99	100.34	0.99	580
10	1.99	99.77	0.99	326

Next, inversion is performed with three, six, seven, and nine unknown parameters by tabu and SA. The results are, then, compared.

4.1 Simulated Annealing

SA [7, 8, 9, 10] is an optimization process which is widely used for source localization and geoacoustic inversion. The idea behind SA is essentially obtained from statistical mechanics. Assume that we expose a solid to a very high temperature, so that the solid melts and all atoms circulate in a random fashion. Next, the temperature of the liquid is reduced gradually so that all atoms arrange themselves in the minimum energy state where crystallization takes place. In optimization, this energy is directly related to our optimizing function. SA is the simulation of this annealing process; the method searches for the global minimum energy level of E, where E equals $1 - F$ (F is the matched field correlation). Notice that minimization of E corresponds to maximization of F.

Starting with an initial temperature T_0 and an initial model $\mathbf{m_0}$ associated with an initial energy E_0, the temperature is reduced slowly so that the process converges to the globally minimum energy state. In each iteration, SA finds a new model $\mathbf{m_1}$ with energy E_1 by perturbing the current model $\mathbf{m_0}$. The perturbation is generated as $m_{1i} = m_{0i} + \Delta m_i \gamma$ where γ is chosen randomly in (-1,1), i corresponds to the i-th element of the model $\mathbf{m}$, and Δm_i is a fixed number associated with the bounds for the i-th parameter perturbation. If the energy E (1-F) is lowered by this new parameter change ($\Delta E = E_0 - E_1 < 0$), then this new model $\mathbf{m_1}$ is accepted unconditionally. Otherwise, $\mathbf{m_1}$ is accepted with probability $\mathbf{P} = exp(-\frac{\Delta E}{T_i})$, where T_i is the temperature at the current iteration. This process is repeated until the change of energy ΔE becomes negligibly small for several iterations; then, convergence of the process has been achieved. In 1984, Geman and Geman [30] proved that if the

temperature cooling schedule follows a logarithmic pattern, then SA in theory could converge to the global minimum. The logarithmic schedule is given below for $i \geq 2$:

$$T(i) = \frac{T_0}{ln(i)} \tag{4.1}$$

This convergence, however, also requires "appropriate" choices for the parameter perturbations and also for the initial temperature.

4.2 Fast Simulated Annealing

Although the convergence of SA to the global minimum (global maximum in our case) by using the logarithmic schedule is theoretically guaranteed (if the temperature schedule and parameter perturbations are appropriate), SA is very slow and takes a significant amount of time until its convergence to the global minimum. Also, sometimes, the global minimum is not identified in practice. In 1987, Szu and Harley [12] presented a fast simulated annealing algorithm, where the temperature schedule is inversely proportional to the iteration number:

$$T(i) = \frac{T_0}{i} \tag{4.2}$$

This approach has been used in matched-field inversion with success. Based on this fact, we have also used a fast SA schedule. Parameter perturbations are performed as $m_{1i} = m_{0i} + \Delta m_i \gamma^3$ [31], where γ is chosen randomly in the interval (-1,1). This approach encourages small parameter perturbations, without prohibiting bigger variability [31].

4.3 Results and Discussions

4.3.1 3D Inversion

For a comparison between SA and tabu, we perform three-dimensional inversion with 15 sets of initial conditions. The true parameter values are provided in Table 4.2. For the appropriate annealing schedule, we have experimented with several different temperature schedules. In order to have a high performance bound for tabu, we tried to find a schedule so that SA finds the global maximum at the true location most of the time.

Table 4.2 The True Values of the Parameters and the Bounds on Parameters : x_s = Range, z_s = Source Depth, od_s = Ocean Depth

No	Parameters	True	Minimum	Maximum
1	x_s - km	2.0	0.01	5.0
2	$z_s - m$	100.0	0.0	200.0
3	$od_s - m$	216.5	200.0	230.0

Once the appropriate schedule was found, we performed an efficiency test for three-dimensional inversion. The value of the global maximum is 1 (perfect match), and it occurs at the true location. Therefore, for this comparison, we accept that a method is successful if it reaches within 10% of the global maximum value. In other words, the maximum obtained by each process in every run needs to exceed a threshold, which is 0.90 in our case. A process is said to be more efficient than the other one, if it requires fewer forward model calculations to exceed the given threshold value than the other method. The number of forward model calculations is here defined as the number of times normal modes are calculated. The minimum number of models is fixed for each process. However, if a method does not satisfy this criterion within the pre-defined number of models, the number of models is increased until the process is successful or the process exhausts the maximum allowable number

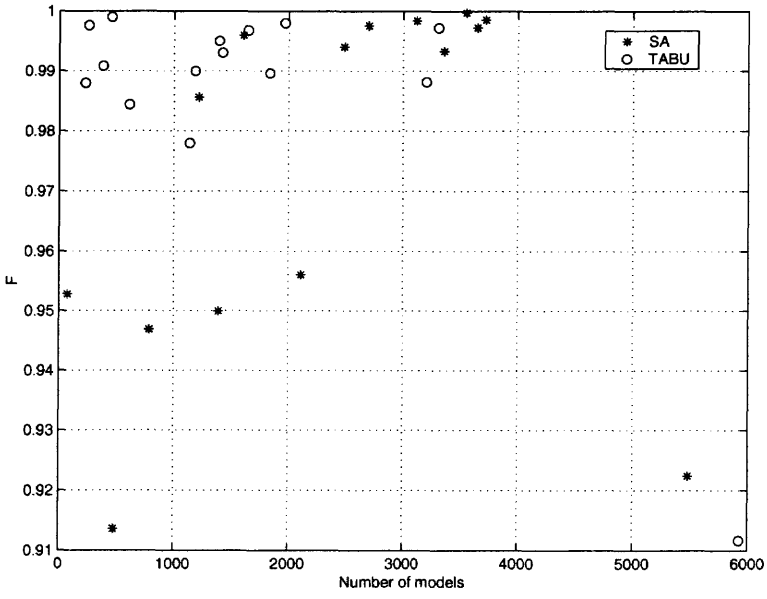

Figure 4.2 Comparison between SA and tabu for 3-D inversion.

of models. If a process does not find a maximum value which exceeds the given threshold value, we consider it as a failure. Table 4.3 presents the efficiency test results for both processes.

Table 4.3 Comparison Between SA and Tabu (3D): Efficiency Test

Process	Mean	Std	Mean(F)	Failure
SA	2382	1475	0.97	0
Tabu	1664	1518	0.99	0

For the three-dimensional inversion, tabu is faster than SA nine out of fifteen times. On average, tabu needs 718 fewer forward model calculations than SA. Also, as we observe in the table, tabu reaches a higher value of the optimizing function than SA. Figure 4.2 presents the number of models versus maximum for both methods. This figure clearly indicates that tabu obtains higher maxima more efficiently than SA. Tabu obtains maxima higher than 0.98 eleven out of fifteen times within 2000

forward model calculations, whereas SA reaches this level twice within the same number of calculations.

We also obtain the mean and standard deviations of the estimates obtained by each process if the estimates are associated with the true source location. As we have mentioned in Chapter 3, source range and depth are the most important parameters. Tilt and ocean depth are the next significant parameters. Since all other remaining parameters do not affect the optimizing function significantly, obtaining mean and standard deviations of these parameters do not provide us with substantial information. Table 4.4 presents the mean and standard deviations of significant parameters. The numbers in parentheses represent the corresponding standard deviations. Both methods perform similarly.

Table 4.4 Comparison Between SA and Tabu (3D)

Parameter	Tabu	SA
r	2.01(0.02)	1.99(0.05)
sd	99.97(0.61)	99.93(2.07)
od	217.26(0.93)	216.37(2.44)

4.3.2 6D Inversion

Next, the search is extended by considering sediment thickness, receiver shift, and array tilt as unknown parameters as well. From the sensitivity plots in Chapter 3, one can see that tilt is an important parameter affecting the optimizing function significantly. Shift does not appear to be as significant as tilt; however, both tilt and shift could be unknown or uncertain in a realistic application. Figure 4.1 shows such a case. Also, typically, sediment parameters are uncertain in shallow water problems, and they should, thus, be included in the inversion.

The environment is the same as the one used for the three-dimensional inversion. The true parameter values of the six considered parameters are provided in Table 4.5.

Table 4.5 The True Values of the Parameters and the Bounds on Parameters : x_s = Range, z_s = Source Depth, od_s = Ocean Depth, sed_{thick} = Sediment Thickness, sh = Receiver Shifts, ti = Array Tilt

No	Parameters	True	Minimum	Maximum
1	x_s - km	2.0	0.01	5.0
2	$z_s - m$	100.0	0.0	200.0
3	$od_s - m$	216.5	200.0	230.0
4	sed_{thick} - m	23.5	5.0	145.0
5	sh - m	0.0	-5.0	5.0
6	ti - degree	0.0	-5.0	5.0

Table 4.6 provides the information for our comparison based on efficiency. Tabu is faster than SA ten out of fifteen times. On average, tabu needs approximately 6000 fewer forward model calculations than SA. Also, again, higher maxima are identified by tabu than by SA. The number of models versus maximum for the six-dimensional inversion is presented in Figure 4.3. We notice that tabu obtains maxima higher than 0.97 ten out of fifteen times within 20000 forward model calculations, whereas SA exceeds this level only once within the same number of calculations.

Table 4.6 Comparison Between SA and Tabu (6D): Efficiency Test

Process	Mean	Std	Mean(F)	Failure
SA	16188	7293	0.94	0
Tabu	10385	7136	0.97	0

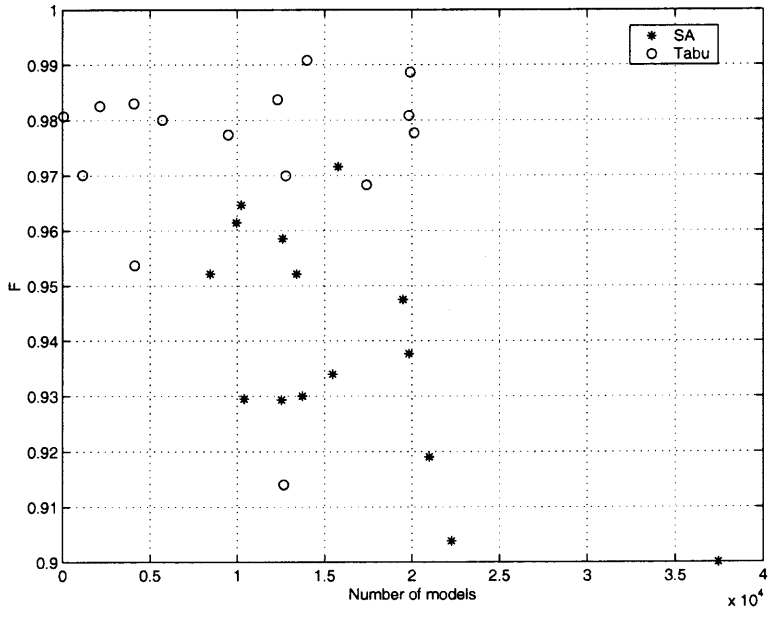

Figure 4.3 Comparison between SA and tabu for 6-D inversion.

The mean and standard deviations of the estimates are provided in Table 4.7. Although both methods perform well, tabu estimates tilt and ocean depth more accurately than SA.

Table 4.7 Comparison Between SA and Tabu (6D)

Parameter	Tabu	SA
r	2.01(0.09)	2.04(0.1)
sd	99.99(2.46)	101.87(2.54)
od	216.88(4.86)	219.15(5.6)
ti	-0.02(0.09)	0.27(0.35)

4.3.3 7D Inversion

The dimensionality of the parameter space is extended to seven, by adding attenuation to the problem. Table 4.8 lists the true parameter values for the inversion.

Table 4.8 The True Values of the Parameters and the Bounds on Parameters : x_s = Range, z_s = Source Depth, od_s = Ocean Depth, sed_{thick} = Sediment Thickness, sh = Receiver Shifts, ti = Array Tilt, att = Attenuation

No	Parameters	True	Minimum	Maximum
1	x_s - km	2.0	0.01	5.0
2	$z_s - m$	100.0	0.0	200.0
3	$od_s - m$	216.5	200.0	230.0
4	sed_{thick} - m	23.5	5.0	145.0
5	sh - m	0.0	-5.0	5.0
6	ti - degree	0.0	-5.0	5.0
7	att - (dB/m kHz)	0.2	0.0	1

SA and tabu are then compared for the seven-dimensional estimation problem. Tabu is faster than SA eleven out of fifteen times. On average, tabu needs 9703 fewer forward model calculations than SA to exceed the threshold. Also, as before, tabu attains a higher optimizing function value than SA (see Figure 4.4). Tabu obtains maxima higher than 0.97 nine out of fifteen times within 30000 forward model calculations, whereas, within the same number of model calculations, SA never attains this level.

Table 4.9 Comparison Between SA and Tabu (7D): Efficiency Test

Process	Mean	Std	Mean(F)	Failure
SA	31890	7606	0.96	0
Tabu	22186	15767	0.97	0

Table 4.10 shows that SA obtains slightly better estimates for source location parameters and ocean depth.

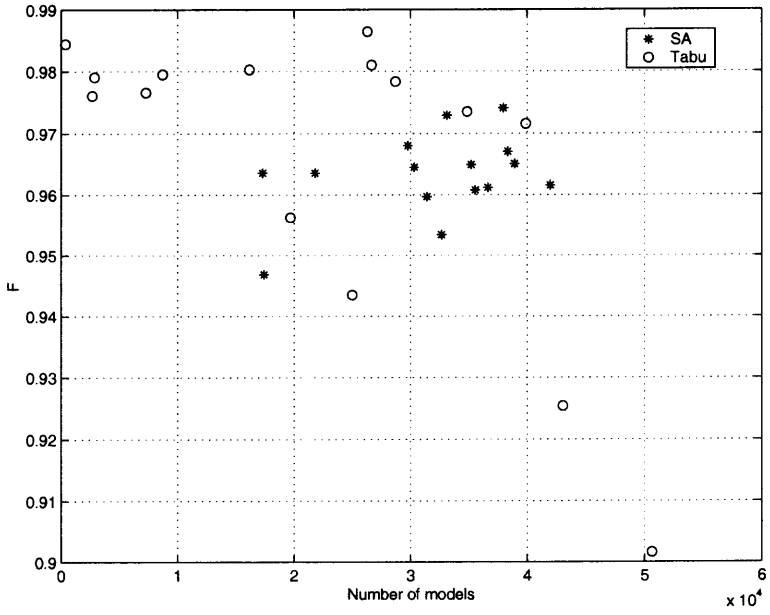

Figure 4.4 Comparison between SA and tabu for 7-D inversion.

Table 4.10 Comparison Between SA and Tabu (7D)

Parameter	Tabu	SA
r	1.95(0.1)	2.04(0.1)
sd	98.44(2.75)	100.97(2.69)
od	213.6(5.33)	218.73(5.14)
ti	0.06(0.21)	0.07(0.23)

4.3.4 9D Inversion

The search is, then, extended to nine dimensions by adding sound speed at the top and bottom interfaces of the sediment as unknown parameters. The true parameter values are provided in Table 4.11.

Table 4.11 The True Values of the Parameters and the Bounds on Parameters : x_s = Range, z_s = Source Depth, od_s = Ocean Depth, sed_{thick} = Sediment Thickness, sh = Receiver Shifts, ti = Array Tilt, att = Attenuation, ssp1 = Sound Speed 1, ssp2 = Sound Speed 2

No	Parameters	True	Minimum	Maximum
1	x_s - km	2.0	0.01	5.0
2	$z_s - m$	100.0	0.0	200.0
3	$od_s - m$	216.5	200.0	230.0
4	sed_{thick} - m	23.5	5.0	145.0
5	sh - m	0.0	-5.0	5.0
6	ti - degree	0.0	-5.0	5.0
7	att - (dB/m kHz)	0.2	0.0	1
8	ssp1 - (m/sec)	1572.368	1530.0	1630.0
7	ssp2 - (m/sec)	1593.016	1550.0	1650.0

The efficiency test results are shown in Table 4.12. On average, tabu needs approximately 13000 fewer forward model calculations than SA. Also, tabu provides significantly higher maxima than SA (see Figure 4.5). For the nine-dimensional case, SA does not exceed the threshold value once. Table 4.13 shows that tabu obtains better estimates for source range, depth, and ocean depth.

The following should be noted here. For the seven-dimensional case, we notice that tabu identifies the main lobe eleven out of fifteen times within 45000 number of models whereas, SA identifies it fifteen out of fifteen times. However, we find that

Table 4.12 Comparison Between SA and Tabu (9D): Efficiency Test

Process	Mean	Std	Mean(F)	Failure
SA	35931	17879	0.93	1
Tabu	22824	14348	0.98	0

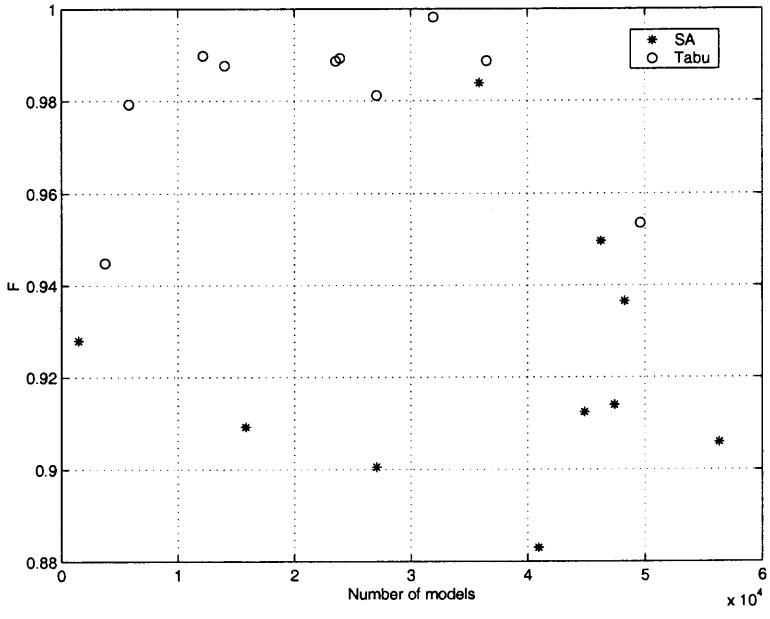

Figure 4.5 Comparison between SA and tabu for 9-D inversion.

Table 4.13 Comparison Between SA and Tabu (9D)

Parameter	Tabu	SA
r	1.99(0.1)	2.07(0.072)
sd	99.51(2.41)	101.57(1.61)
od	216.19(5.45)	220.31(3.47)
ti	-0.06(0.14)	0.02(0.60)

eight out of fifteen times tabu is faster than SA in locating the source. To further investigate tabu, we consider more forward models and observe that tabu identifies the main lobe fourteen out of fifteen times afterwards. Tabu still has a lower average number of forward models (27013) and higher maxima (0.98) than SA.

Since, for all above mentioned inversion processes, tabu requires fewer forward model calculations than SA to exceed the optimizing function threshold, we conclude that tabu is more efficient than SA. In three-dimensional inversion, both methods estimate the parameters well. However, in six and nine-dimensional inversion, tabu provides consistently better estimates for the source location parameters and the ocean depth. Tabu also provides higher average maxima than SA in all above mentioned examples. Thus, we conclude that tabu, on average, provides better estimates than SA.

Next, we provide an example of nine-dimensional inversion by tabu (see Figure 4.6). The accumulation of dots almost everywhere in plots, provided for sediment thickness, shift, attenuation, and sound speeds, show that the optimizing function is relatively insensitive to these parameters.

Finally, we have generated a surface from source range and depth values explored by tabu for the nine-dimensional inversion by using interpolation; this is presented in Figure 4.7. Here, we only consider the source range and depth. This figure clearly indicates the correct source location. The values of the optimizing function are significantly higher in this region than the other regions.

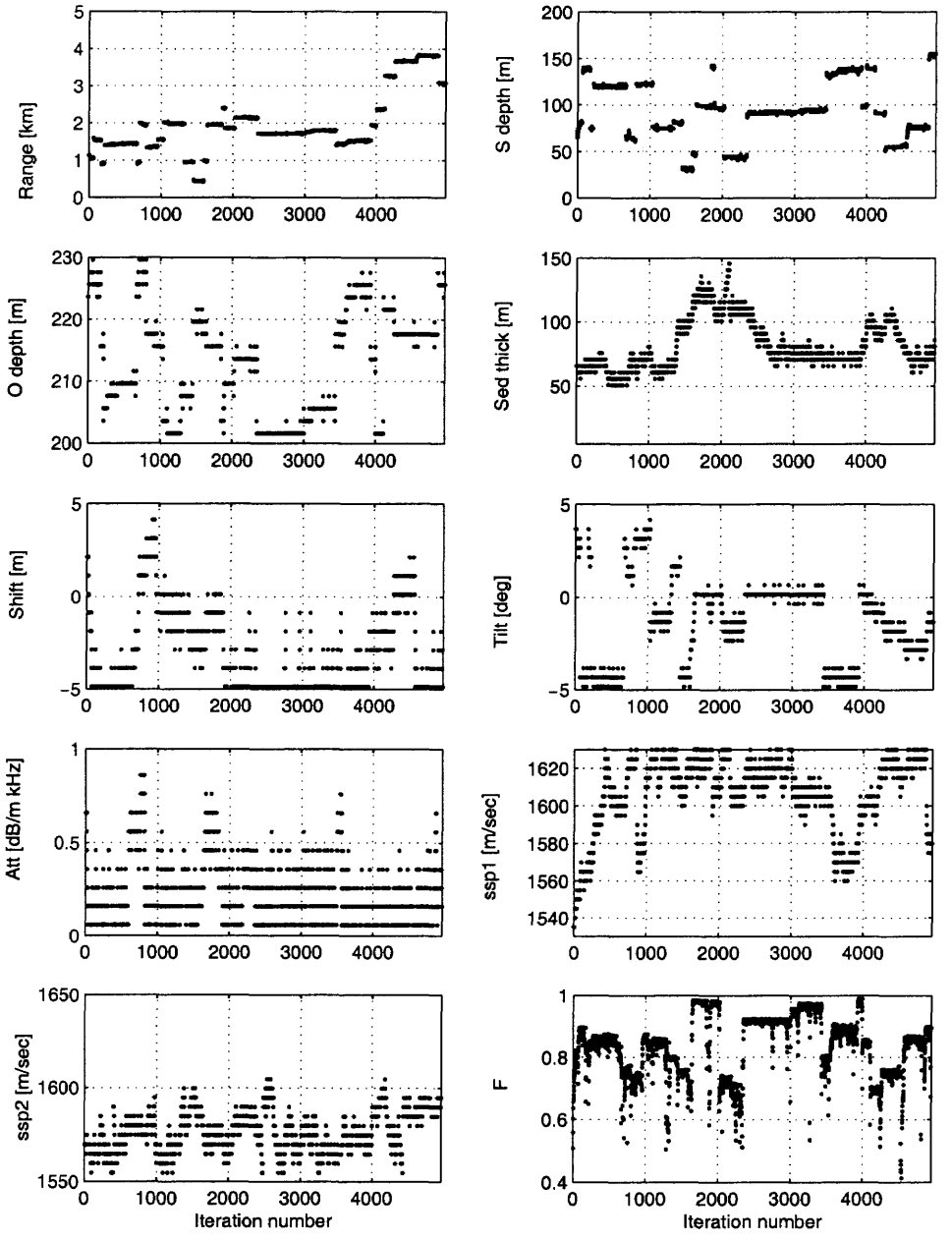

Figure 4.6 An example of tabu search for nine-dimensional inversion.

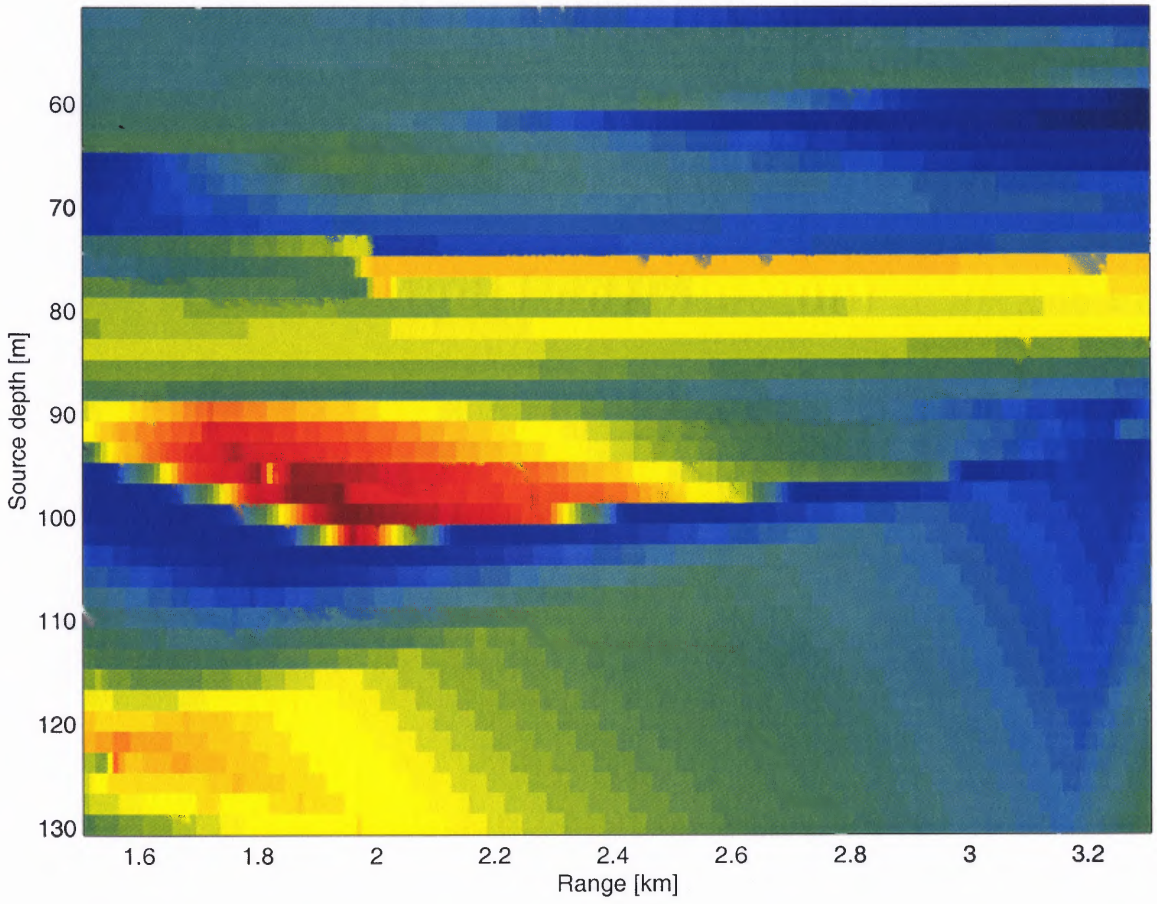

Figure 4.7 Surface obtained from source range and depth values visited by tabu for nine-dimensional inversion.

CHAPTER 5

REPARAMETRIZATION

Recently, rotation of coordinates has received considerable attention in optimization for underwater acoustic inversion [25, 17, 18, 24]. The idea behind this technique involves exploiting the correlation between different parameters while performing inversion. When parameters are correlated, the high energy models (the models which have high optimizing function values) are often distributed along a line that is obliquely aligned to the regular coordinate axes. Searching the parameter space in the original coordinate system by perturbing one parameter at a time is usually inefficient. Also, since the optimizing function is affected differently by each parameter (see Figure 3.4), finding reliable estimates of the parameters by using a regular optimization method is difficult when a large number of unknown parameters is involved. However, the performance of the search process can be improved by rotating the coordinates so that the new coordinate axes become parallel and perpendicular to the prominent hills of the optimizing function space [25, 17, 18, 24].

Rotation involves finding (linearly independent, orthogonal) eigenvectors of the covariance matrix **Cov** of the gradient of the optimization function F (see Equation 2.3) where **Cov** is defined as [24, 25] $\mathbf{Cov} = \int_\Omega \bigtriangledown F(\bigtriangledown F)^t d\Omega$ and Ω consists of dimensionless bounds of all parameters. Each element of **Cov** can be written as:

$$Cov_{ij} = \int_\Omega \frac{\partial F}{\partial x_i}\frac{\partial F}{\partial x_j} d\Omega \tag{5.1}$$

where x_i and x_j are the i-th and j-th normalized parameters.

The information obtained from this covariance matrix is useful for efficient inversion. The eigenvectors correspond to the rotated axes of the inversion [25, 24]. The parameter associated with the largest eigenvalue of **Cov** is the most important parameter for the estimation process.

Inversion is performed in rotated coordinates as follows: all parameters x_i are non-dimensionalized by dividing each parameter by the total bound allowed for it. **Cov** is calculated by using Monte Carlo integration [32]. For the integration, a set of discrete points is chosen randomly from the parameter space and for each of these points, $\frac{\partial F}{\partial x_i}$ is estimated as follows:

$$\frac{\partial F}{\partial x_i} = \frac{F(x_i + \Delta x_i) - F(x_i - \Delta x_i)}{2\Delta x_i} \tag{5.2}$$

where Δx_i is the dimensionless step size for the i-th parameter x_i. The convergence of the Monte Carlo scheme for three, six, seven, and nine-dimensional cases is studied and demonstrated in Figures 5.1 to 5.4. For all cases, Monte Carlo integration is performed for 120, 320 and 420 points. Parameters 1 to 9 correspond to range, source depth, ocean depth, sediment thickness, shift, tilt, attenuation, sound speed 1, and sound speed 2, respectively. In the figures, the uppermost plot shows the convergence of the most important eigenvector which is associated with the largest eigenvalue, the next one corresponds to the convergence of the eigenvector associated with the second largest eigenvalue and so on. For different numbers of random points, the elements of each eigenvector could differ but usually not significantly. However, the rankings of the parameters based on their importance remain unchanged. In all of these plots, the parameters are ranked as follows: source range, source depth, tilt, ocean depth, sediment thickness, shift, sound speed 1, attenuation, and sound speed 2.

In Figure 5.1, in the first eigenvector we notice that the elements corresponding to source range and ocean depth have the largest values; this is an indication of coupling between them. Similarly, in the same figure, we observe that coupling exists between the range, depth, and the ocean depth (third eigenvector). In all convergence plots, we notice that coupling exists between range and ocean depth (see the first eigenvector), between ocean depth and tilt (see the third eigenvector, which is more

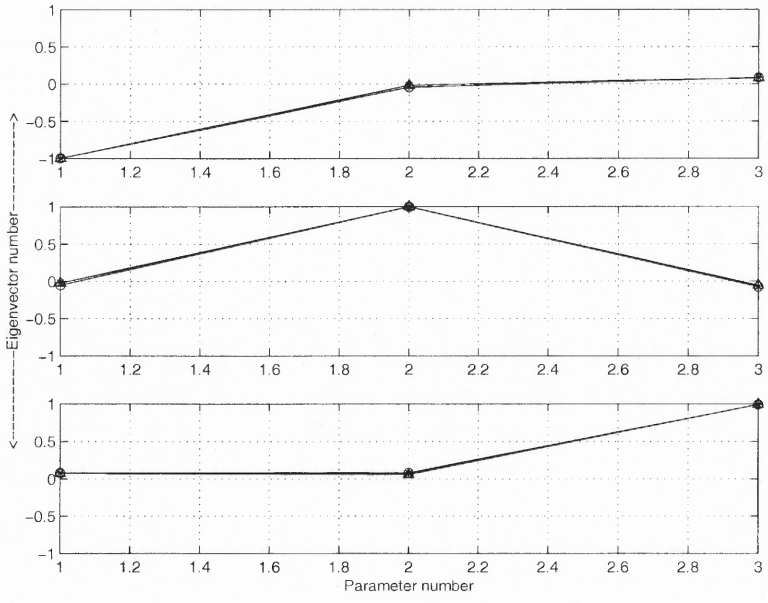

Figure 5.1 Comparison of eigenvectors obtained for three-dimensional inversion when 120 (circles), 320 (star) and 420 (hat) points are used in the Monte Carlo integration. The eigenvectors are ranked in terms of significance, the top plot corresponding to the most significant eigenvector.

prominent in Figure 5.2), between ocean depth, receiver shifts (see the fourth and sixth eigenvectors), and so on.

A comparison of eigenvalues is also presented in Figure 5.5. Each eigenvalue e is divided by the largest eigenvalue e_1, and, then, these values are presented in logarithmic scale. We observe that the eigenvalues associated with the source location parameters are significantly larger than those corresponding to the other parameters.

Once the Monte Carlo integration is performed and the eigenvectors are obtained for the rotated coordinates, tabu is implemented with reparametrization.

5.1 Tabu in Rotated Coordinates

While searching the parameter space with tabu in rotated coordinates, in each iteration a local neighborhood is created by perturbing all vectors as follows:

$$\hat{\mathbf{x}} = \mathbf{x} \pm k_j \mathbf{v_j} \tag{5.3}$$

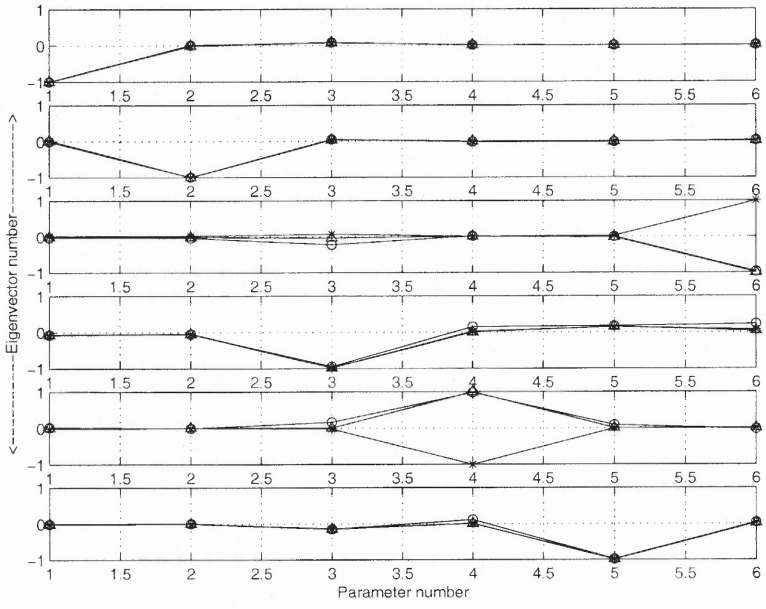

Figure 5.2 Comparison of eigenvectors obtained for six-dimensional inversion when 120 (circles), 320 (star) and 420 (hat) points are used in the Monte Carlo integration. The eigenvectors are ranked in terms of significance, the top plot corresponding to the most significant eigenvector.

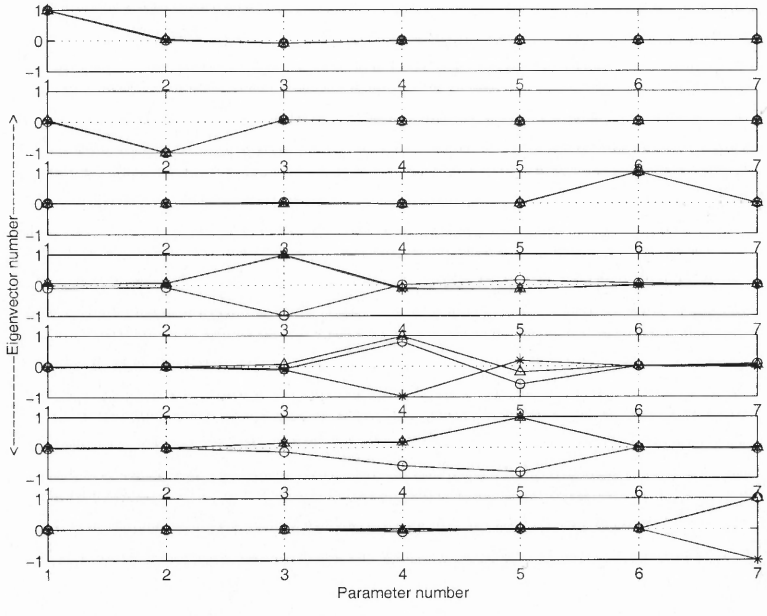

Figure 5.3 Comparison of eigenvectors obtained for seven-dimensional inversion when 120 (circles), 320 (star) and 420 (hat) points are used in the Monte Carlo integration. The eigenvectors are ranked in terms of significance, the top plot corresponding to the most significant eigenvector.

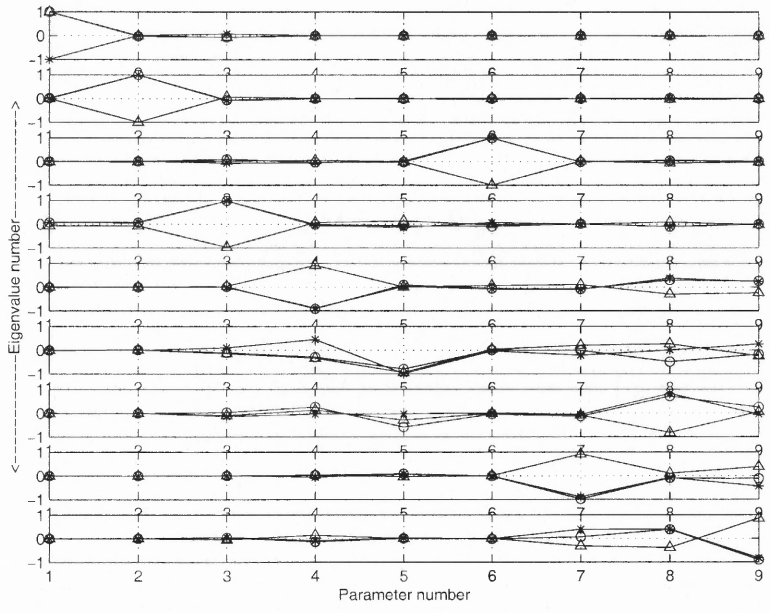

Figure 5.4 Comparison of eigenvectors obtained for nine-dimensional inversion when 120 (circles), 320 (star), 420 (hat) points are used in Monte Carlo integration. The eigenvectors are ranked in terms of significance, the top plot corresponding to the most significant eigenvector.

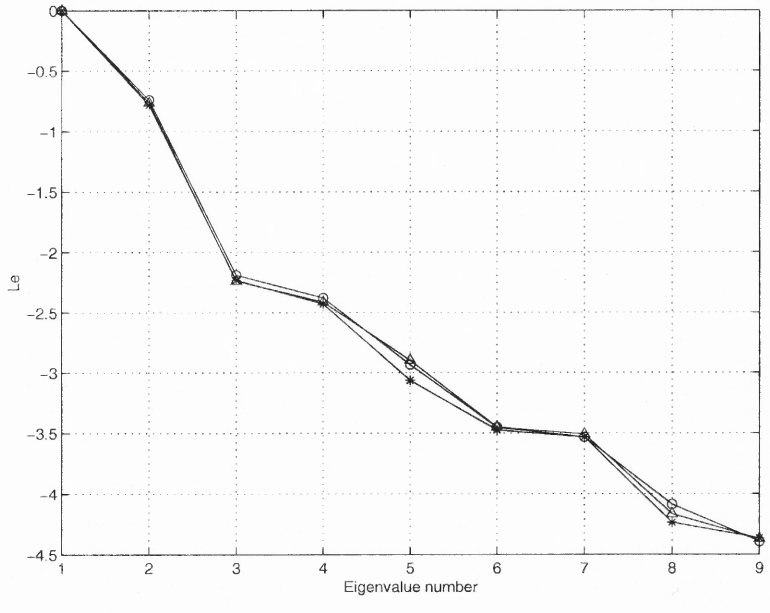

Figure 5.5 Comparison of eigenvalues obtained for nine-dimensional inversion when 120 (circles), 320 (star), and 420 (hat) points are used in the Monte Carlo integration; $Le = log_{10}(\frac{e}{e_1})$ where e_1 = the largest eigenvalue, the eigenvalues e are shown in a logarithmic scale from the largest to the smallest, from top to bottom, respectively.

where $\hat{\mathbf{x}}$ is the new dimensionless model, $\mathbf{x}$ is the old dimensionless model, k_j is a scalar multiple chosen in an automated way for the j-th eigenvector. The scalar k_j is selected in such a way that the parameter value associated with the largest value in the j-th eigenvector does not exceed the original step size that was used for tabu in the original coordinates. Once the new dimensionless model $\hat{\mathbf{x}}$ is obtained, this model is transformed to the conventional coordinate system, and the search is performed using the corresponding values of the unknown parameter.

Only those two eigenvectors which are associated with the first two largest eigenvalues are perturbed when tabu jumps out of a confinement. To keep the number of forward model calculations to a minimum, we neglect all other less significant eigenvectors when a trap is identified. However, once tabu escapes, we perturb all eigenvectors again, as shown in Equation 5.3.

Next we perform inversion by tabu and SA in original and rotated coordinates.

5.2 Results and Discussions: Tabu in Original Coordinates and Tabu in Rotated Coordinates.

5.2.1 3D Inversion

Table 5.1 Comparison Between Tabu and Tabu(Rotated) (3D): Efficiency Test

Process	Mean	Std	Mean(F)	Failure
Tabu	1664	1518	0.99	0
Tabu(Rotated)	1700	1546	0.99	0

We compare tabu in original coordinates with tabu in rotated coordinates. Table 5.1 provides the three-dimensional inversion results by both processes, when we test efficiency. We notice that the regular tabu search requires fewer number of forward model calculations than the reparametrized tabu.

5.2.2 6D Inversion

Next, the two methods are compared for six-dimensional inversion. Table 5.2 demonstrates the inversion results for efficiency test. We observe that tabu in rotated coordinates requires fewer forward model calculations than tabu in conventional coordinates. Here, both methods attain the same level of maxima.

Table 5.2 Comparison Between Tabu and Tabu(Rotated) (6D): Efficiency Test

Process	Mean	Std	Mean(F)	Failure
Tabu	10385	7136	0.97	0
Tabu(Rotated)	10066	7252	0.97	0

5.2.3 7D Inversion

We continue inversion by assuming that seven parameter values are unknown. We observe in Table 5.3 that the reparametrized tabu needs fewer forward model calculations than the regular tabu search. Again both methods obtain similar maxima.

Table 5.3 Comparison Between Tabu and Tabu(Rotated) (7D): Efficiency Test

Process	Mean	Std	Mean(F)	Failure
Tabu	22186	15767	0.97	0
Tabu(Rotated)	20611	10399	0.97	0

5.2.4 9D Inversion

Inversion is, then, performed for nine unknown parameters. Table 5.4 shows the efficiency test results for both tabu processes. Tabu in regular coordinates requires fewer forward model calculations and it also reaches slightly higher maxima.

We notice that tabu in regular coordinates provides higher or same level of maxima in all cases. Thus, we conclude that tabu, on average, is able to obtain higher

Table 5.4 Comparison Between Tabu and Tabu(Rotated) (9D): Efficiency Test

Process	Mean	Std	Mean(F)	Failure
Tabu	22824	14348	0.98	0
Tabu(Rotated)	24855	13860	0.96	0

correlation than tabu in rotated coordinates. However, this is not surprising. Since tabu in conventional coordinates searches the space by perturbing one parameter at a time, the search has the ability to penetrate deep inside a neighborhood. Tabu in rotated axes searches the space by perturbing all parameters simultaneously. Unless we use smaller step sizes, tabu in rotated axes could be less accurate than tabu in regular coordinates.

We also present an example of nine-dimensional inversion by tabu in rotated axes in Figure 5.6. These results are obtained by using the same initial conditions as those used for the regular tabu method (see Figure 4.6). The surface generated by these solutions is presented in Figure 5.7. We observe more high correlation regions in this figure than what was observed for the case of regular tabu, as previously shown in Figure 4.7. This is not surprising since tabu in rotated axes is expected to identify more high peak areas than it does in conventional coordinates.

Finally, to show how tabu in rotated axes provides better estimates for the less important parameters, we present histograms obtained from solutions by using both methods for a fixed number of forward model calculations. Histograms for the three-dimensional case show that both methods obtain good estimates for all parameters (see Figure 5.8). Histograms for the six-dimensional case (see Figures 5.9 and 5.10) show that tabu in conventional coordinates obtains better estimates for source range, source depth, and tilt. However, tabu in rotated coordinates obtains better estimates for ocean depth and sediment thickness. Histograms provided for seven-dimensional inversion (see Figures 5.11 and 5.12) indicate that although both

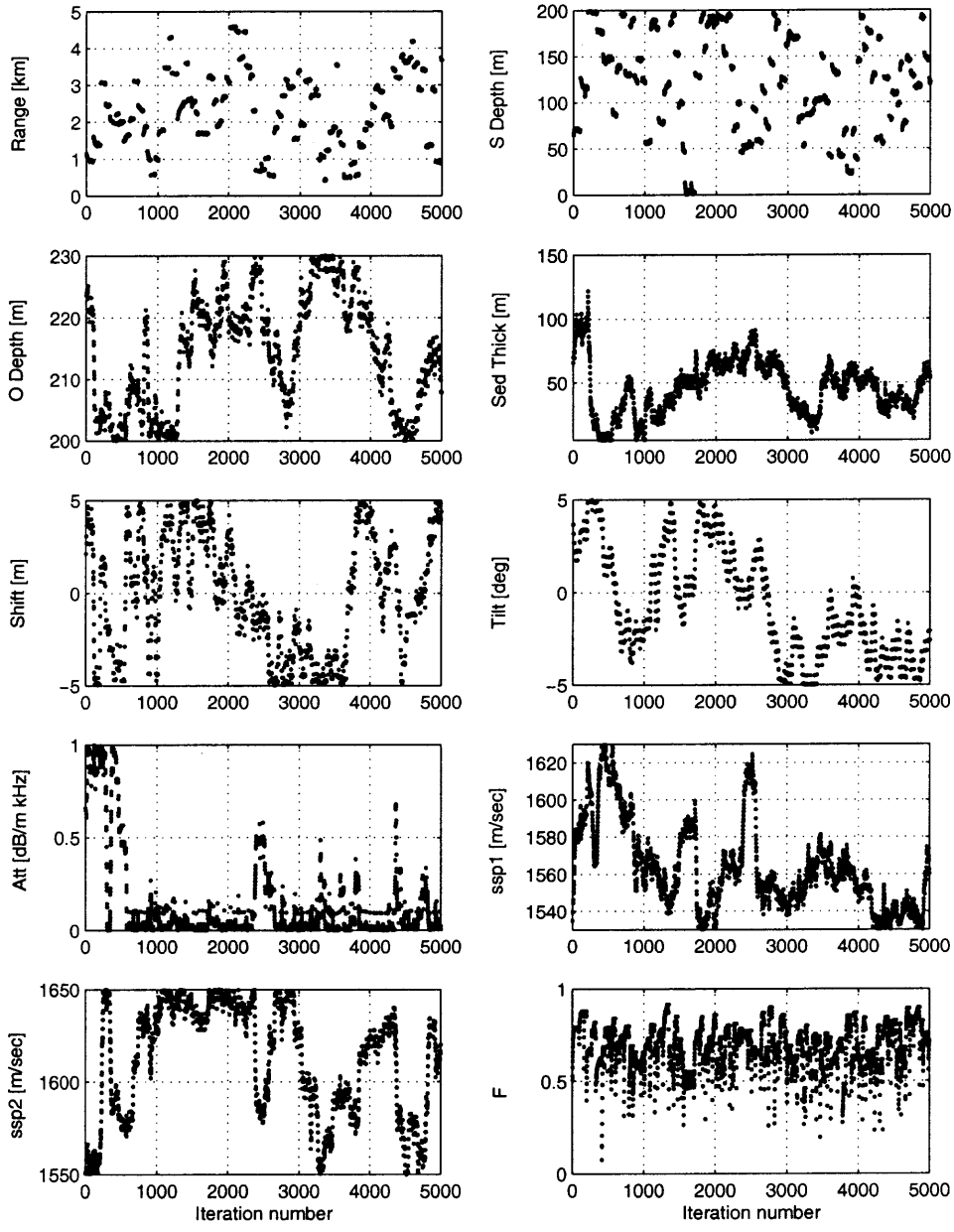

Figure 5.6 An example of nine-dimensional inversion by tabu(Rotated).

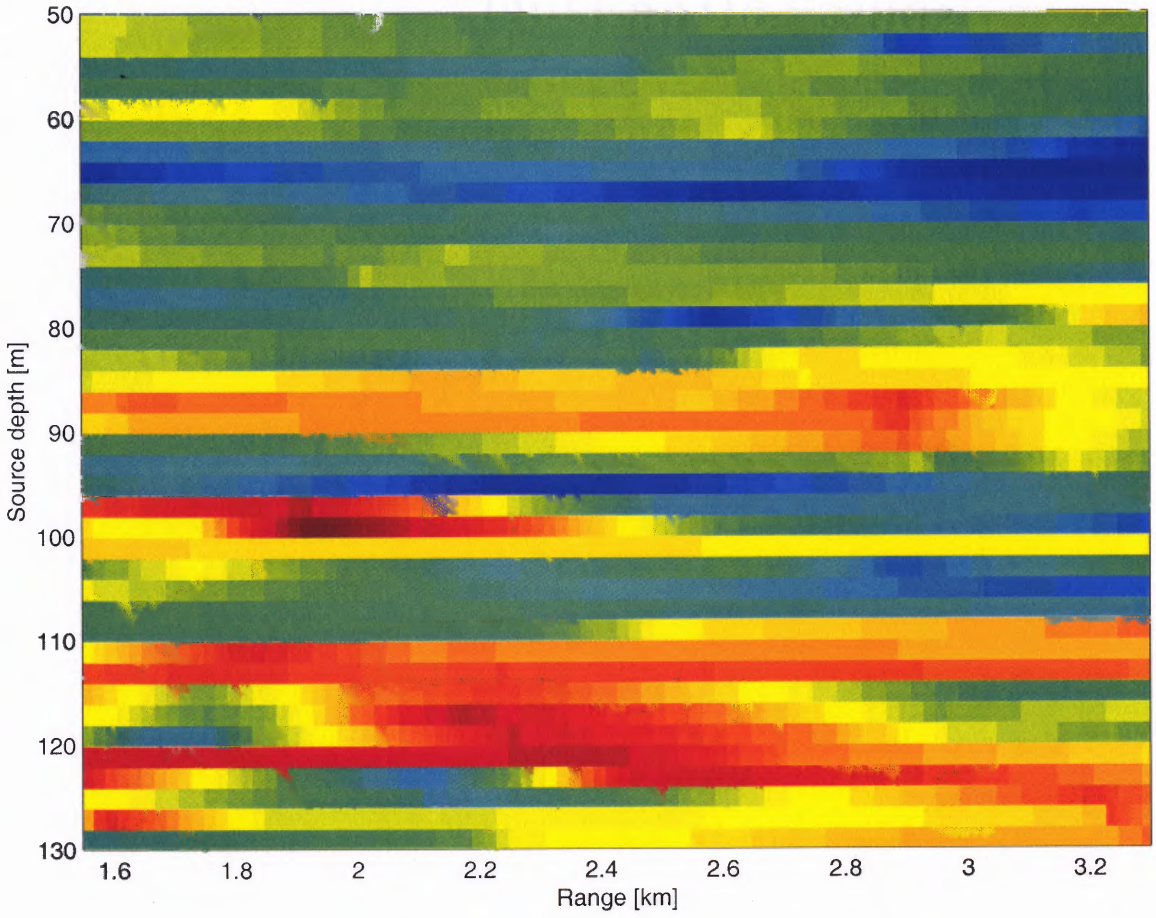

Figure 5.7 Surface obtained from source range and depth values visited by tabu in rotated coordinates.

methods perform well in estimation of source location, tabu in rotated axes obtains better estimates for source range, whereas tabu in conventional coordinates produces better estimates for source depth. In addition, ocean depth, tilt, and attenuation are better estimated by tabu in rotated axes. In nine-dimensional inversion (see Figures 5.13 and 5.14), tabu in rotated coordinates provides better estimates for range, tilt and sound speed 1; regular tabu produces better estimates for source depth. Both methods perform in a similar manner for estimation of ocean depth. Therefore, it is observed, that tabu in rotated coordinates provides more reliable estimates for less important parameters than the regular tabu approach.

However, we were surprised because we did not see a gain in terms of efficiency with the reparametrized tabu compared to the regular tabu method. Existing literature informs us that a search in rotated coordinates typically performs better than the corresponding regular method. After a careful consideration, we realize that using the normal mode method for forward modeling helps tabu to save many forward model calculations, which is the reason behind our results.

5.2.5 Savings from Normal Modes

As we have mentioned earlier, the number of forward model calculations is based on the number of times normal modes are calculated. Using a modal approach, we are able to use the same modes obtained for a given environment to calculate the field (p in Chapter 2) simultaneously for all location parameters. In normal modes, the modal solutions ($\chi_m(z)$ in Equation 2.2) are obtained by using a specific set of environmental parameter values.

Once these modes are obtained for a specific environment, any solution ($p(x, z_s)$ in Equation 2.2) can be represented as a linear combination of these modes, provided the environmental conditions are same. Consequently, if there are unknown parameter values associated with the source/receiver locations, the normal modes which are

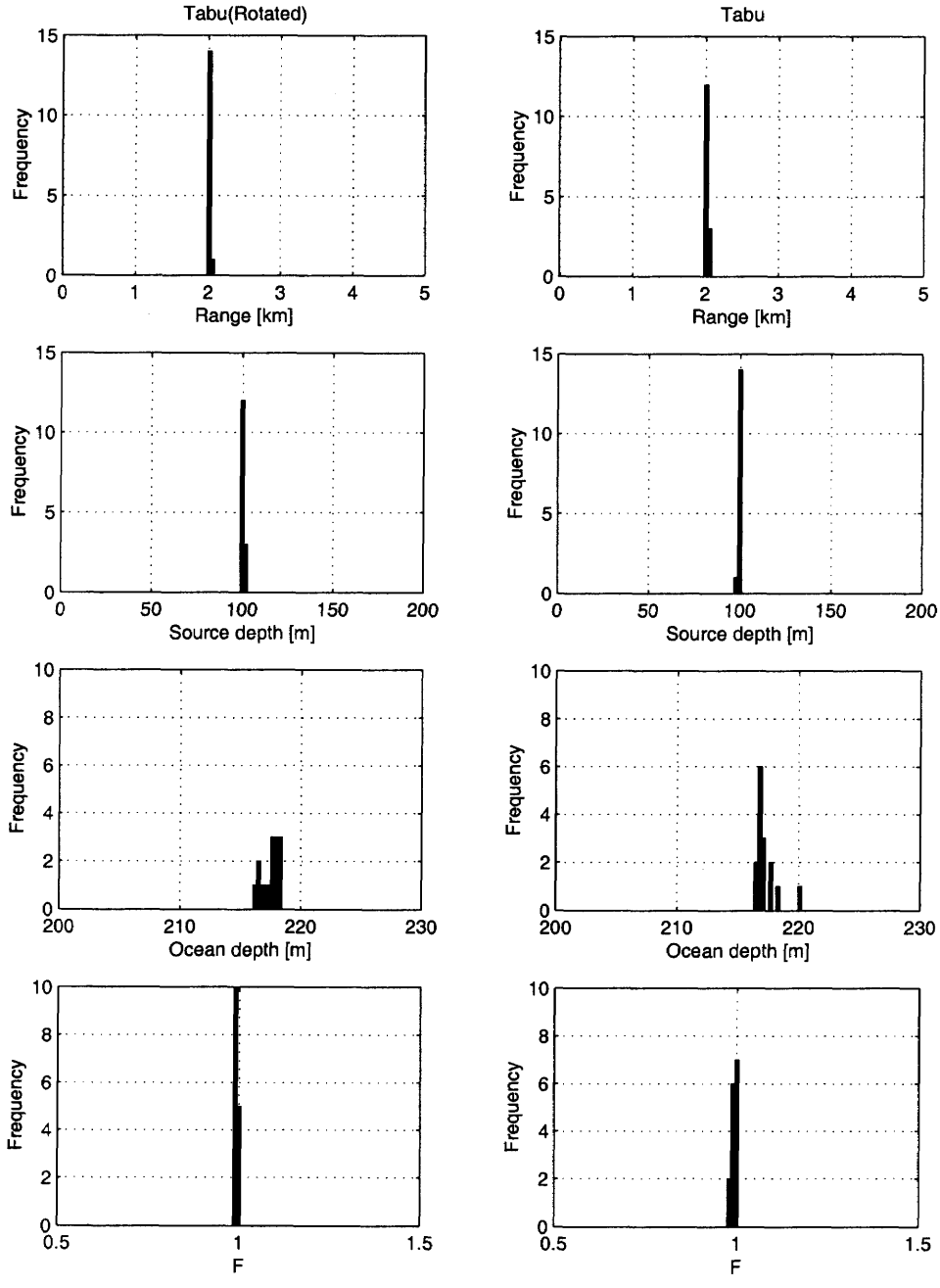

Figure 5.8 Histograms for three-dimensional inversion.

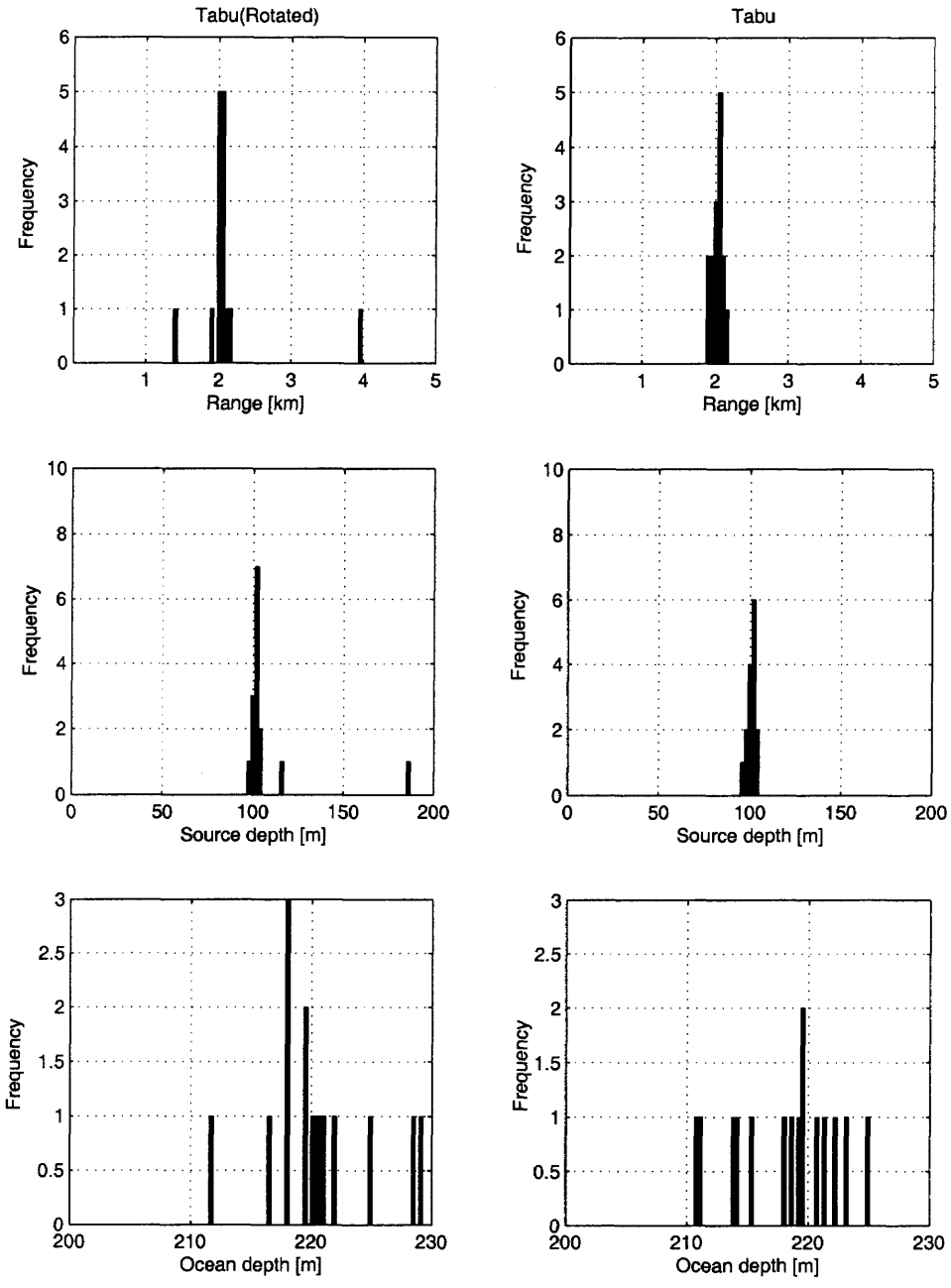

Figure 5.9 Histograms for six-dimensional inversion.

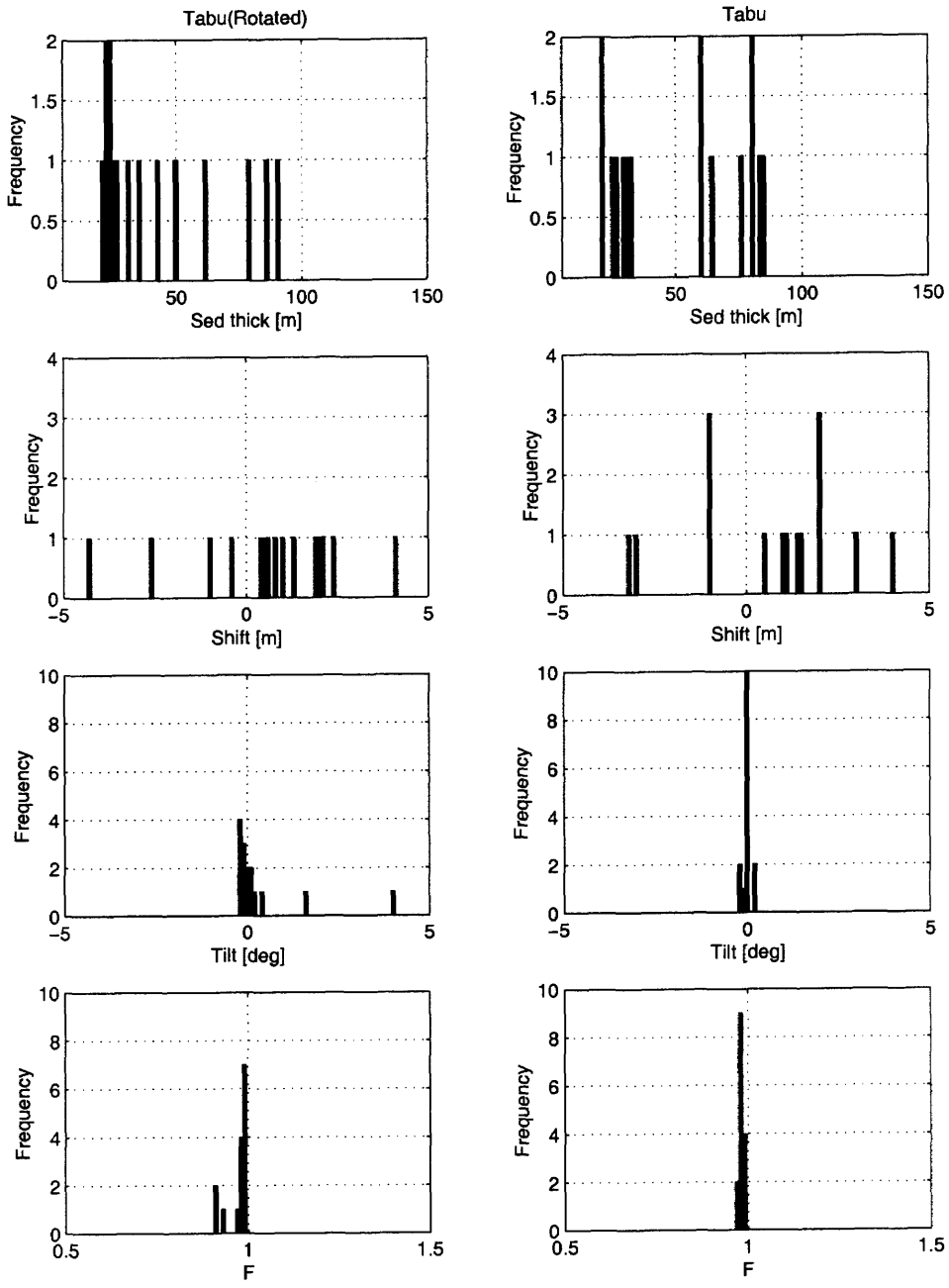

Figure 5.10 Histograms for six-dimensional inversion.

already obtained, can be used to obtain the pressure fields (p in Chapter 2) for all source/receiver location parameter values (x, z_s, z), provided the environment is the same; thus, a significant number of forward model calculations could be avoided.

When we use regular tabu, in every iteration each neighborhood model is different from the previously found best model by only one parameter value. As an illustration, consider the three-dimensional problem. The true values of the source range, depth, and water column depth are assumed to be unknown. When a neighborhood of size $2(unk - par)$ is created, four models in this neighborhood have the same environmental parameter values as the best model had in the previous iteration. Therefore, the modes obtained for the previous model are used for field calculations corresponding to these four models. As a consequence, four forward model calculations are saved. Similarly, eight forward model calculations for the six-dimensional problem (two environmental parameters and four source/receiver location parameters) and eight forward model calculations for the seven-dimensional problem (three environmental parameters and four source/receiver location parameters) could be saved with the regular tabu method per iteration. With tabu in rotated coordinates, since the eigenvectors are perturbed (see Equation 5.3), all parameter values change simultaneously. Thus, the search is under-privileged compared to the regular tabu search when many source/receiver location parameters are among the unknowns. Consider the three and six-dimensional cases where the number of source/receiver location parameters is twice the number of environmental parameters. Each time this method perturbs an eigenvector and converts the perturbed eigenvector in the regular coordinate system, all parameter values are changed, including those of the environmental parameters. Consequently, reparametrized tabu needs to recalculate the normal modes every time an eigenvector is perturbed.

However, if the number of unknown environmental parameter values is higher than the number of source/receiver location parameter values, tabu with reparametri-

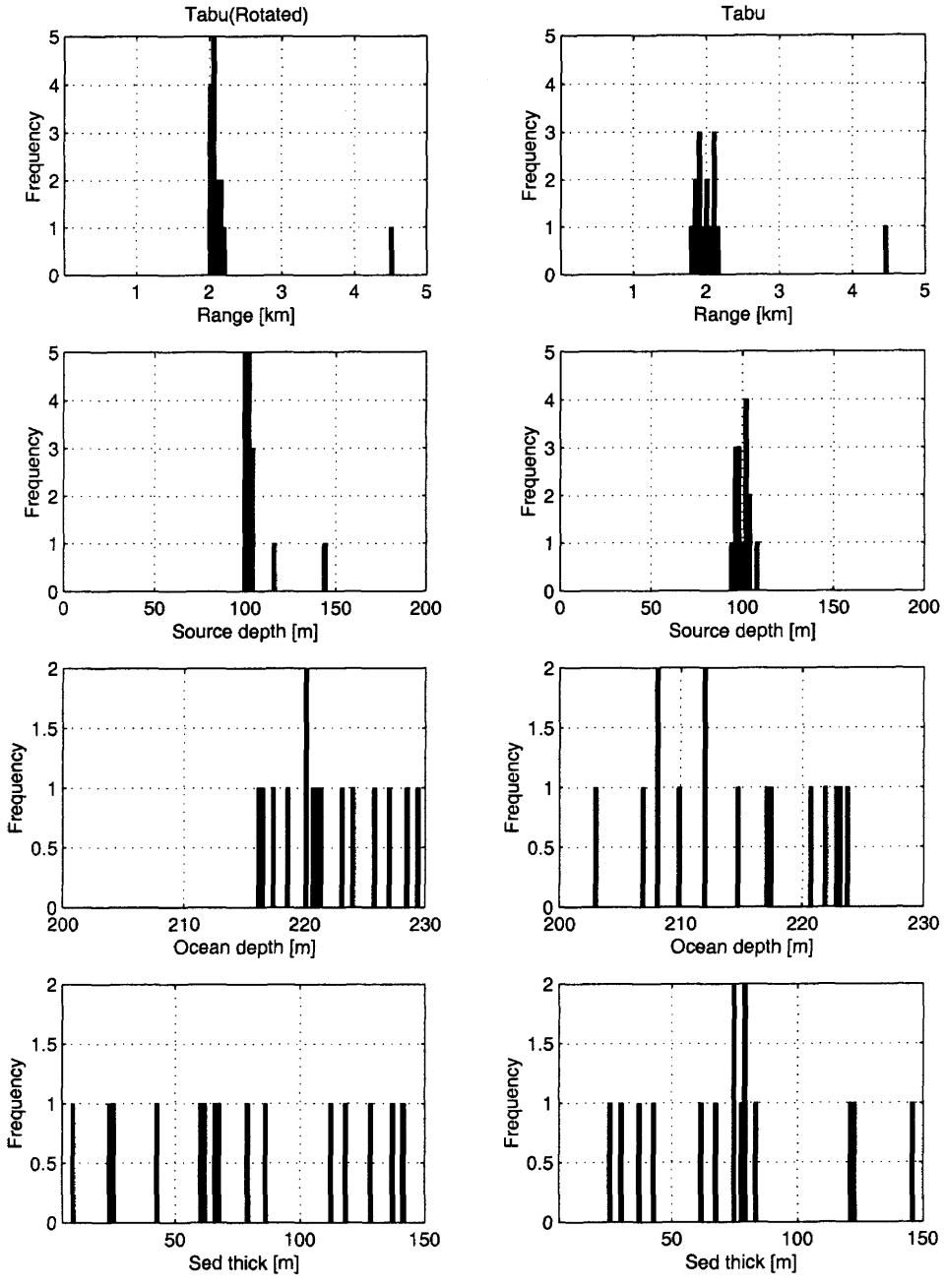

Figure 5.11 Histograms for seven-dimensional inversion.

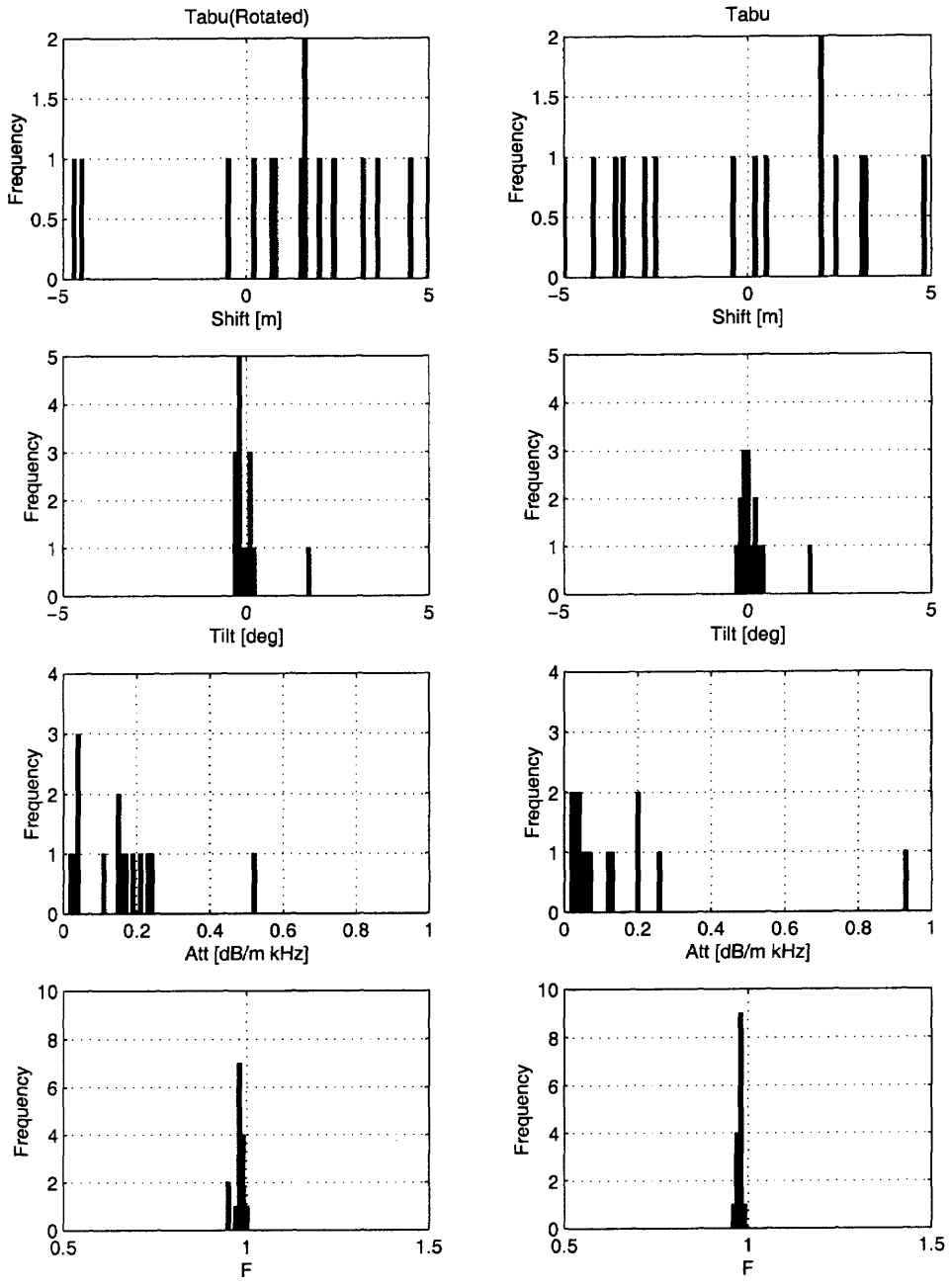

Figure 5.12 Histograms for seven-dimensional inversion.

zation has higher chances, on average, of finding the true location by calculating fewer number of forward models than the regular tabu method.

To illustrate our reasoning, we compare both processes for three, six, seven and nine-dimensional problems based on iteration numbers. Tables 5.5 to 5.8 present the mean and standard deviations of iteration numbers corresponding to the results obtained from the efficiency test.

Table 5.5 Comparison Between Tabu and Tabu(Rotated) (3D) Based on Iteration Numbers

Process	Mean	Std	Mean(F)	Failure
Tabu	603	537	0.99	0
Tabu(Rotated)	460	425	0.99	0

Table 5.6 Comparison Between Tabu and Tabu(Rotated) (6D) Based on Iteration Numbers

Process	Mean	Std	Mean(F)	Failure
Tabu	3027	2095	0.97	0
Tabu(Rotated)	1338	974	0.97	0

Table 5.7 Comparison Between Tabu and Tabu(Rotated) (7D) Based on Iteration Numbers

Process	Mean	Std	Mean(F)	Failure
Tabu	7273	7659	0.97	0
Tabu(Rotated)	2399	1214	0.97	0

We notice from all these tables that tabu in rotated coordinates requires, on average, fewer iteration numbers than the regular tabu method. Moreover, small standard deviations for all cases for tabu in rotated axes show that the variations

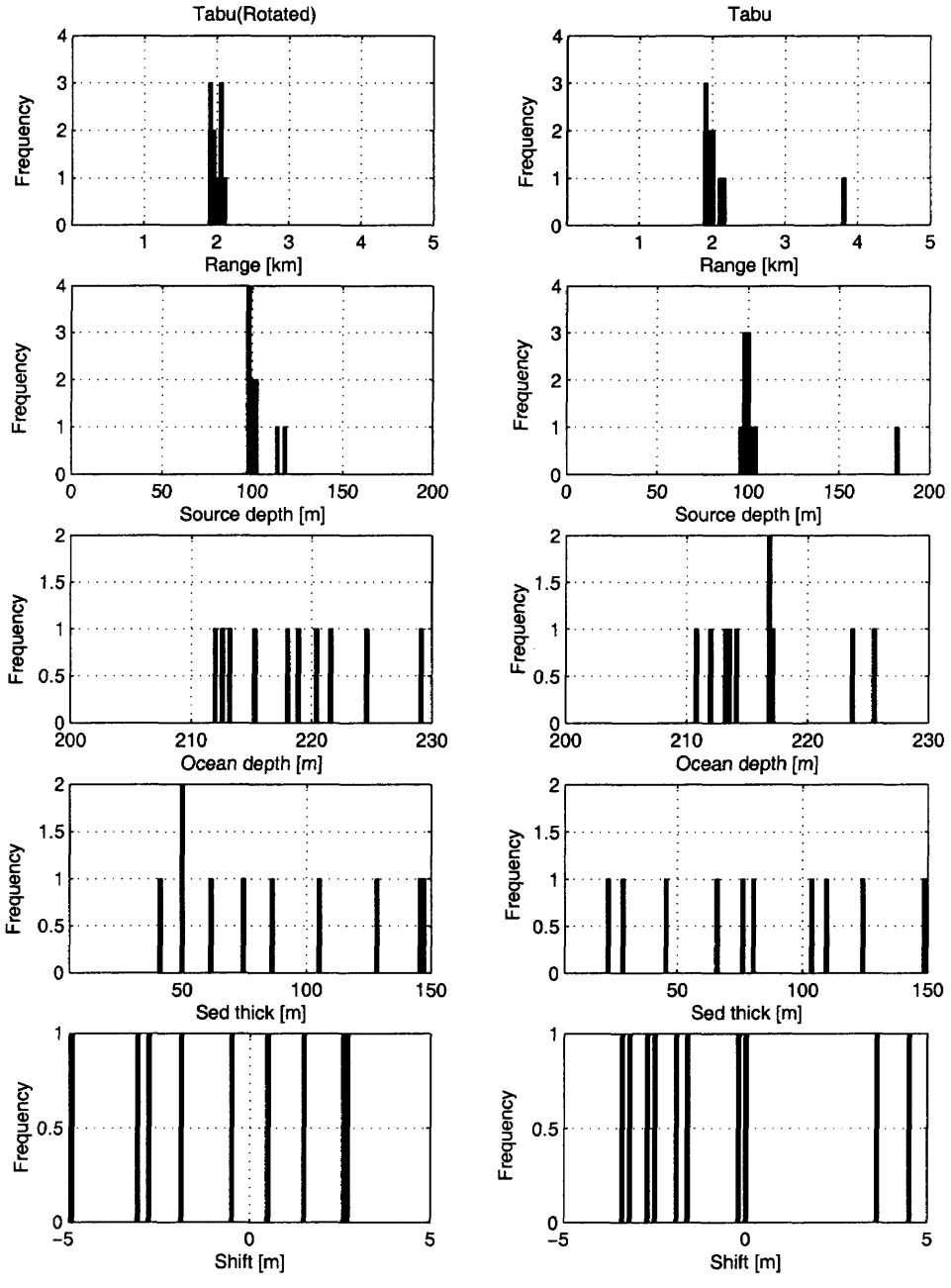

Figure 5.13 Histograms for nine-dimensional inversion.

Table 5.8 Comparison Between Tabu and Tabu(Rotated) (9D) Based on Iteration Numbers

Process	Mean(iter)	Std(iter)	Mean(F)	Failure
Tabu	3607	2241	0.98	0
Tabu(Rotated)	2455	1393	0.96	0

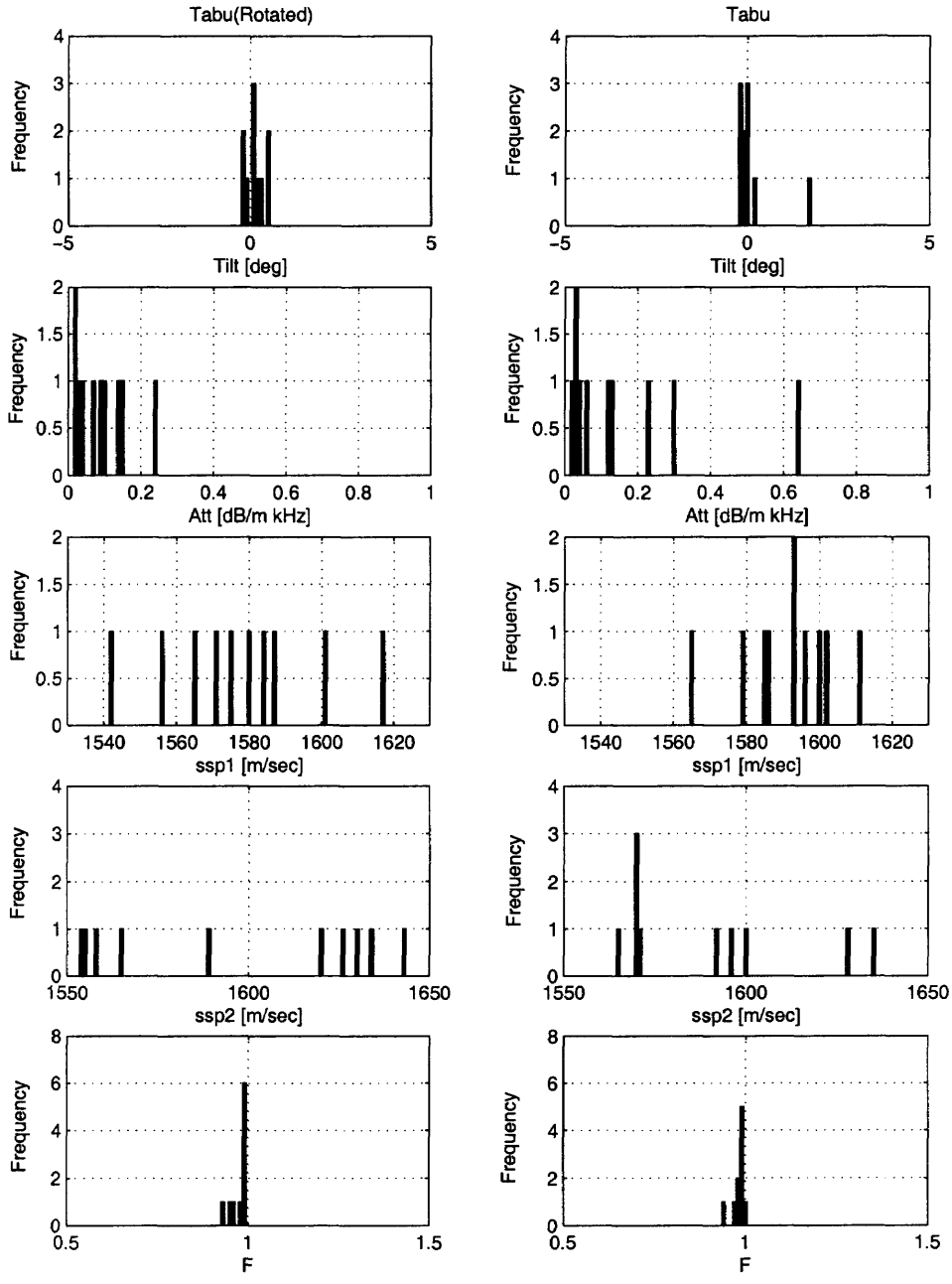

Figure 5.14 Histograms for nine-dimensional inversion.

from the mean are small for this process. Also, since in realistic situations broadband information is involved, all these savings are multiplied by the number of frequencies; if there are n frequencies involved, to calculate the pressure field (p in Chapter 2) at a specific receiver location, the normal modes need to be calculated n times.

Once tabu is implemented in rotated coordinates, we compare results with SA in rotated coordinates as well. However, before we provide the comparison, we compare the regular SA with SA in rotated coordinates briefly.

5.3 SA in Rotated Coordinates

While implementing SA in rotated coordinates, in each iteration of the inversion process a single eigenvector is perturbed before the temperature is reduced. The current value of the dimensionless parameter is obtained as follows [24]:

$$\tilde{\mathbf{x}} = \mathbf{x} + \frac{1}{2}\gamma^3 \mathbf{v}_i \tag{5.4}$$

where γ is randomly chosen in (-1,1). The fraction $\frac{1}{2}$ is used based on [33]. The temperature schedule is the one used for fast SA in original coordinates.

5.4 Results and Discussion: SA in Rotated Coordinates versus SA in Original Coordinates

5.4.1 3D Inversion

The results for testing efficiency are shown in Table 5.9. On average, SA in rotated coordinates requires more forward model calculations than the corresponding method in regular coordinates. SA in rotated coordinates provides higher maxima than SA in regular coordinates.

Table 5.9 Comparison Between SA and SA(Rotated) (3D): Efficiency Test

Process	Mean	Std	Mean(F)	Failure
SA	2382	1475	0.97	0
SA(Rotated)	2889	1042	0.99	0

5.4.2 6D Inversion

SA in rotated coordinates requires fewer forward model calculations than the corresponding SA method in the regular coordinate system for six-dimensional inversion. Table 5.10 presents these results. Also, reparametrized SA finds higher average maxima than the regular SA method.

Table 5.10 Comparison Between SA and SA(Rotated) (6D): Efficiency Test

Process	Mean	Std	Mean(F)	Failure
SA	16188	7293	0.94	0
SA(Rotated)	12110	4297	0.97	0

5.4.3 7D Inversion

As we continue in higher dimensional inversion, we observe that the reparametrized SA is more efficient than the regular SA method and finds higher maxima than the corresponding process in regular coordinates. The results of the efficiency test for seven-dimensional inversion are presented in Table 5.11.

Table 5.11 Comparison Between SA and SA(Rotated) (7D): Efficiency Test

Process	Mean	Std	Mean(F)	Failure
SA	31890	7606	0.96	0
SA(Rotated)	20904	7336	0.96	0

5.4.4 9D Inversion

The efficiency test results for the nine-dimensional inversion are presented in Table 5.12. SA in rotated coordinates requires fewer forward model calculations than the corresponding method in regular coordinates. Also, as usual, this method obtains, on average, higher maxima than regular SA. Notice that SA fails once to satisfy the optimizing function threshold.

Table 5.12 Comparison Between SA and SA(Rotated) (9D): Efficiency Test

Process	Mean	Std	Mean(F)	Failure
SA	35931	17879	0.93	1
SA(Rotated)	29277	14380	0.96	0

5.5 Results and Discussions: Tabu in Rotated Coordinates and SA in Rotated Coordinates

All these results are already obtained and shown previously. However, to compare tabu and SA in rotated coordinates, we include these results in this section as well. Here, SA corresponds to SA in rotated coordinates and tabu corresponds to tabu in rotated axes.

5.5.1 3D Inversion

Table 5.13 provides the efficiency test results for both processes. Tabu in rotated coordinates needs fewer forward model calculations to have a success than SA in the corresponding coordinates for three-dimensional inversion. Both methods obtain same levels of maxima.

Table 5.13 Comparison Between Tabu(Rotated) and SA(Rotated) (3D): Efficiency Test

Process	Mean	Std	Mean(F)	Failure
SA(Rotated)	2889	1042	0.99	0
Tabu(Rotated)	1700	1546	0.99	0

5.5.2 6D Inversion

In six-dimensional inversion, again tabu requires fewer forward model calculations than SA (see Table 5.14). The maxima attained by both processes are same.

Table 5.14 Comparison Between Tabu(Rotated) and SA(Rotated) (6D): Efficiency Test

Process	Mean	Std	Mean(F)	Failure
SA(Rotated)	12110	4297	0.97	0
Tabu(Rotated)	10066	7252	0.97	0

5.5.3 7D Inversion

Table 5.15 presents the results obtained by both processes to test efficiency for seven-dimensional inversion. We notice that tabu requires fewer forward model calculations than SA. Also, on average, tabu obtains higher maxima than SA.

Table 5.15 Comparison Between Tabu(Rotated) and SA(Rotated) (7D): Efficiency Test

Process	Mean	Std	Mean(F)	Failure
SA(Rotated)	20904	7336	0.96	0
Tabu(Rotated)	20611	10399	0.97	0

5.5.4 9D Inversion

As the three and seven-dimensional efficiency test results show, tabu requires fewer forward model calculations than SA for nine-dimensional inversion. The level of maxima found by each process is similar (see Table 5.16).

Table 5.16 Comparison Between Tabu(Rotated) and SA(Rotated) (9D): Efficiency Test

Process	Mean	Std	Mean(F)	Failure
SA(Rotated)	29277	14380	0.96	0
Tabu(Rotated)	24855	13860	0.96	0

To summarize this comparison, tabu is always able to reach the optimizing function threshold by calculating fewer forward models than SA, indicating that tabu is more efficient than SA.

CHAPTER 6

TABU SEARCH WITH REAL DATA

6.1 SWellEX-96 Results

The SWellEX-96 experiment [34, 35, 36, 37] was carried out near San Diego, CA, in May 1996. A brief description of the experiment is presented below.

A source transmits broadband signals with frequencies varying from 200 Hz to 400 Hz. The source is located approximately at 1.1 km in range and 54.6 m in depth. The acoustic signal from the source is received at a vertical line array (VLA). Data are available at 21 hydrophones. This environment is described in a simplified manner in Figure 6.1.

For each frequency, we use the Bartlett processor as it was described in Chapter 2. Since we have broadband information, we average the narrowband ambiguity surfaces as proposed in [38]:

$$B = \frac{\sum_{i=1}^{i=n_{freq}} Log_{10}(F_i)}{n_{freq}} \tag{6.1}$$

where F_i is the output from the Bartlett processor for the $i-th$ frequency and n_{freq} is the number of frequencies involved. Obtaining a geometric mean of the narrowband ambiguity surfaces strengthens the main-lobe of the correlations, suppressing the sidelobes which could lead to erroneous parameter estimation.

We first perform a three-dimensional exhaustive search for 0.01 to 5 km in range, 0 to 100 m of the source depth, and 200 to 230 m in water column depth. This was also performed in [34]. The global maximum (-0.80) is found at 1.04 km for range, 54 m for source depth, and 208.5 m for ocean depth. Although the global maximum occurs approximately at the expected source location, the water column depth is off by 8 m. Due to the complexities involved with the real environment, the global

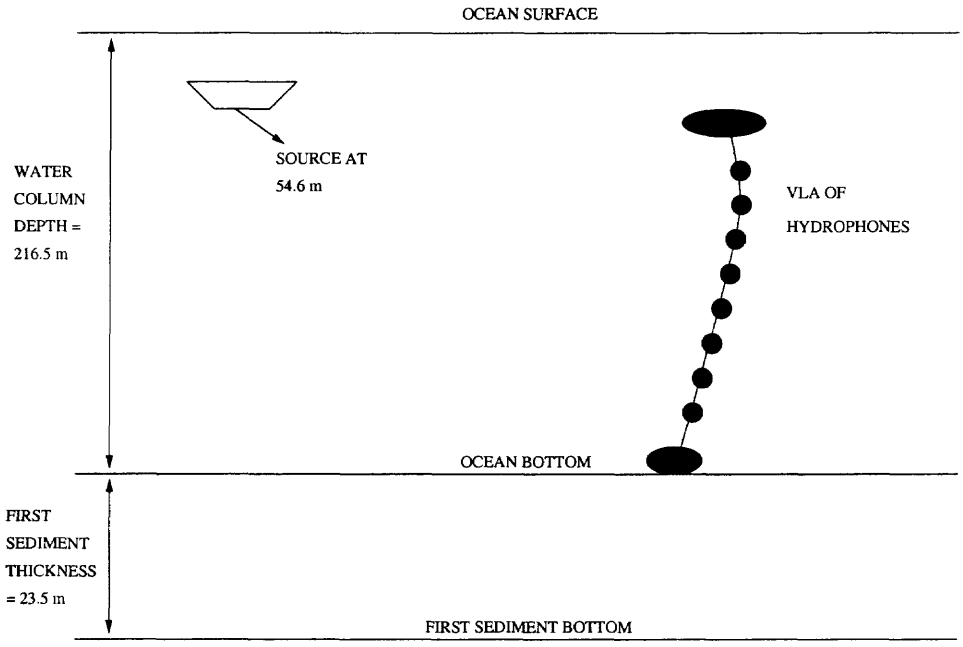

Figure 6.1 A simplified environmental description of SWellEX-96 experiment.

maximum may not occur at the expected parameter values. Figure 6.2 provides the exhaustive search results setting the ocean depth at 208.5 m.

Next, we perform Monte Carlo integration in preparation for three and seven-dimensional inversion in rotated coordinates. The convergence of Monte Carlo integration for the seven-dimensional case is presented in Figure 6.3. Parameters 1 to 7 correspond to range, source depth, ocean depth, sediment thickness, shift, tilt, and attenuation, respectively. The couplings between parameters are different than what we observed in simulations. In Figure 6.3, we observe that range and source depth are correlated (see the first eigenvector), ocean depth and tilt are coupled (see the third eigenvector), ocean depth, receiver shift, and tilt are all correlated (see the fourth eigenvector), sediment thickness and attenuation are coupled (see the sixth and the seventh eigenvectors). Some couplings are more prominent than those we observed in Chapter 5.

The eigenvalues associated with the source location parameters are found to be significantly larger than those of other parameters, as we anticipated (see Figure 6.4).

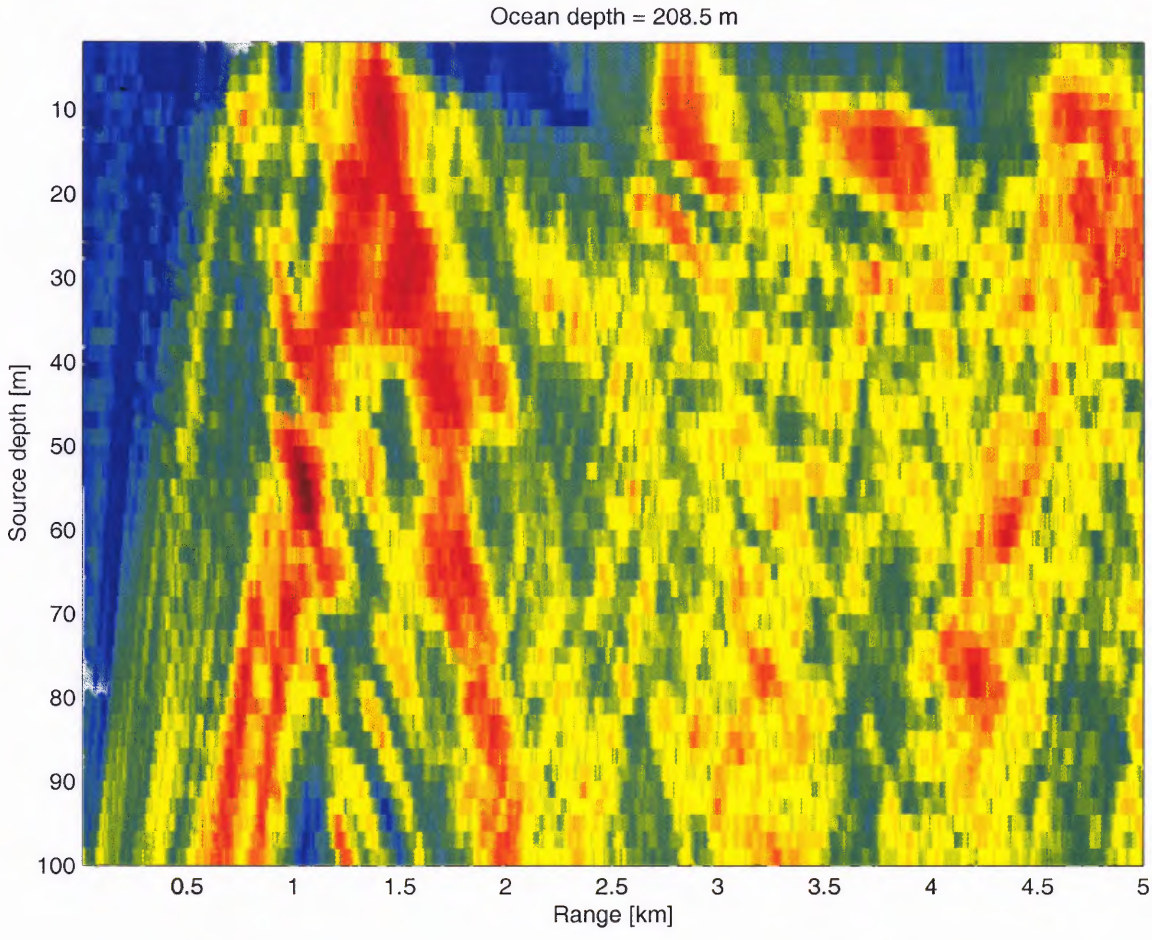

Figure 6.2 Exhaustive search results obtained for ocean depth = 208.5 m.

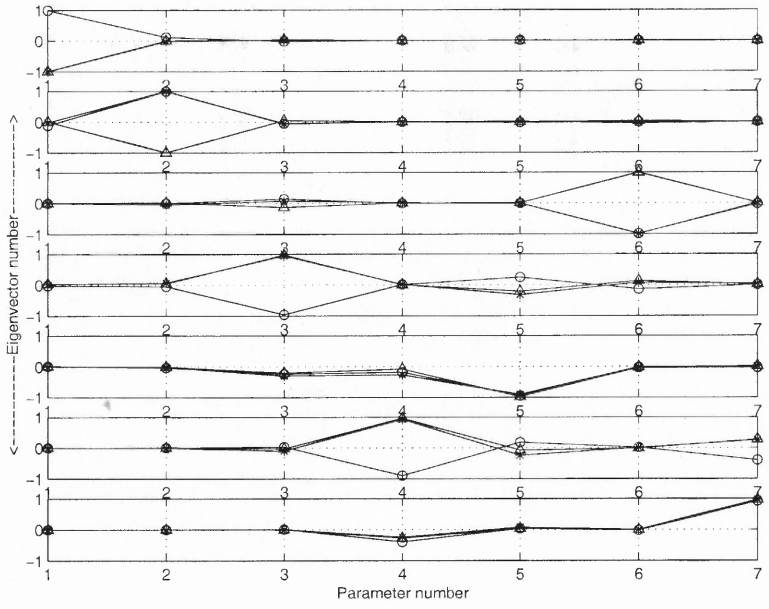

Figure 6.3 Comparison of eigenvectors obtained for seven-dimensional real data inversion when 30 (circles), 60 (star) and 120 (hat) points are used in the Monte Carlo integration. The eigenvectors are ranked in terms of significance, the top plot corresponding to the most significant eigenvector.

In this figure, we also notice that the first four eigenvalues have the same order of significance as seen with the synthetic data. However, the receiver shift becomes more important than the sediment thickness, unlike what we observed in the simulations.

We perform three-dimensional inversion by tabu and tabu in rotated coordinates followed by seven-dimensional inversion. The expected parameter values are shown in Table 6.1.

6.1.1 3D Inversion

For three-dimensional inversion, we present the best solutions obtained from tabu and tabu in rotated coordinates. These results are presented in Table 6.2. We observe that the estimates for the source location and water column depth by both processes match the three-dimensional exhaustive search results. Tabu obtains the maximum earlier than tabu in rotated axes. However, tabu in rotated axes obtains a slightly higher maximum than the regular tabu method. Both methods arrive at the estimates

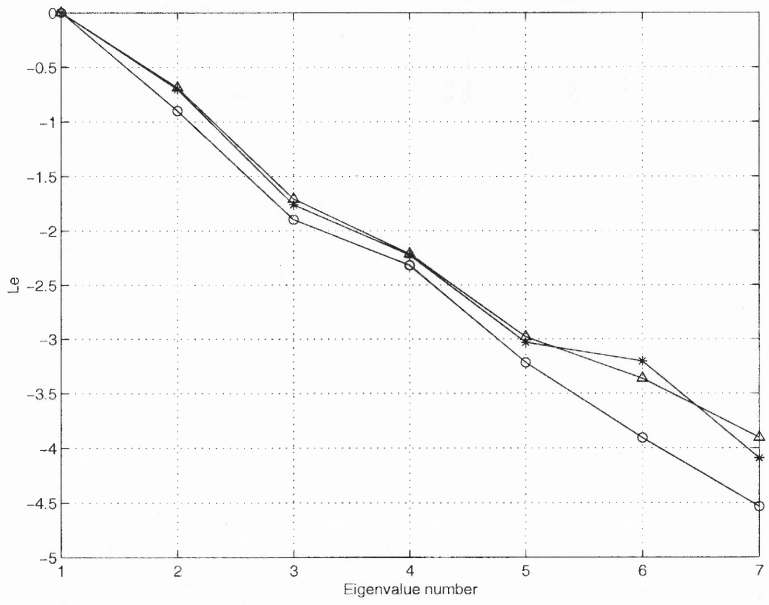

Figure 6.4 Comparison of eigenvalues obtained for seven-dimensional real data inversion when 30 (circles), 60 (star), and 120 (hat) points are used in the Monte Carlo integration; $Le = log_{10}(\frac{e}{e_1})$ where e_1 = the largest eigenvalue, the eigenvalues e are shown in a logarithmic scale from the largest to the smallest, from top to bottom, respectively.

Table 6.1 Expected Values of the Source Location Parameters and Environmental Parameters

No	Parameters	True
1	Source range - km	1.1
2	Source depth - m	54.6
3	Water column depth - m	216.5
4	First sediment thickness - m	23.5
5	Reciver shift - m	unknown
6	Tilt - degree	unknown
7	Attenuation (in first sediment) - (dB/m kHz)	0.2

only after a few calculations. The model numbers which are provided in the sixth column of Table 6.2 represent the number of broadband calculations.

Table 6.2 3D Real Data Inversion

	r	sd	od	F	model
Tabu	1.03	52.55	207.92	-0.81	103
Tabu(Rotated)	1.08	54.78	209.84	-0.80	150

6.1.2 7D Inversion

We have seen earlier that tabu in rotated coordinates provides solutions faster than tabu in conventional coordinates, when several unknown parameters are involved. Therefore, real data inversion is performed here with the reparametrized tabu. Histograms for seven-dimensional inversion are presented in Figure 6.5. We observe that there is a high concentration of estimates in the proximity of the true source location. Moreover, 80% of the estimates for tilt lie between $-2°$ to $2.5°$. The estimates obtained for shift, sediment thickness, ocean depth, and attenuation are more dispersed, because of the optimizing function's relative insensitivity to these four parameters. Table 6.3 presents tabu results obtained from the best solution (highest correlation).

In this table, we notice that the seven-dimensional inversion provides a significantly higher maximum (-0.62) than what we obtained with the three-dimensional exhaustive search (-0.80). The estimates for the source range and depth are found as 1.3 km and 72.93 m respectively, which are different than what we obtained with the three-dimensional exhaustive search. These discrepancies can be explained as follows: the three-dimensional inversion is performed by assuming that tilt is zero. In the seven-dimensional inversion, tilt is found to be nonzero and its estimated value

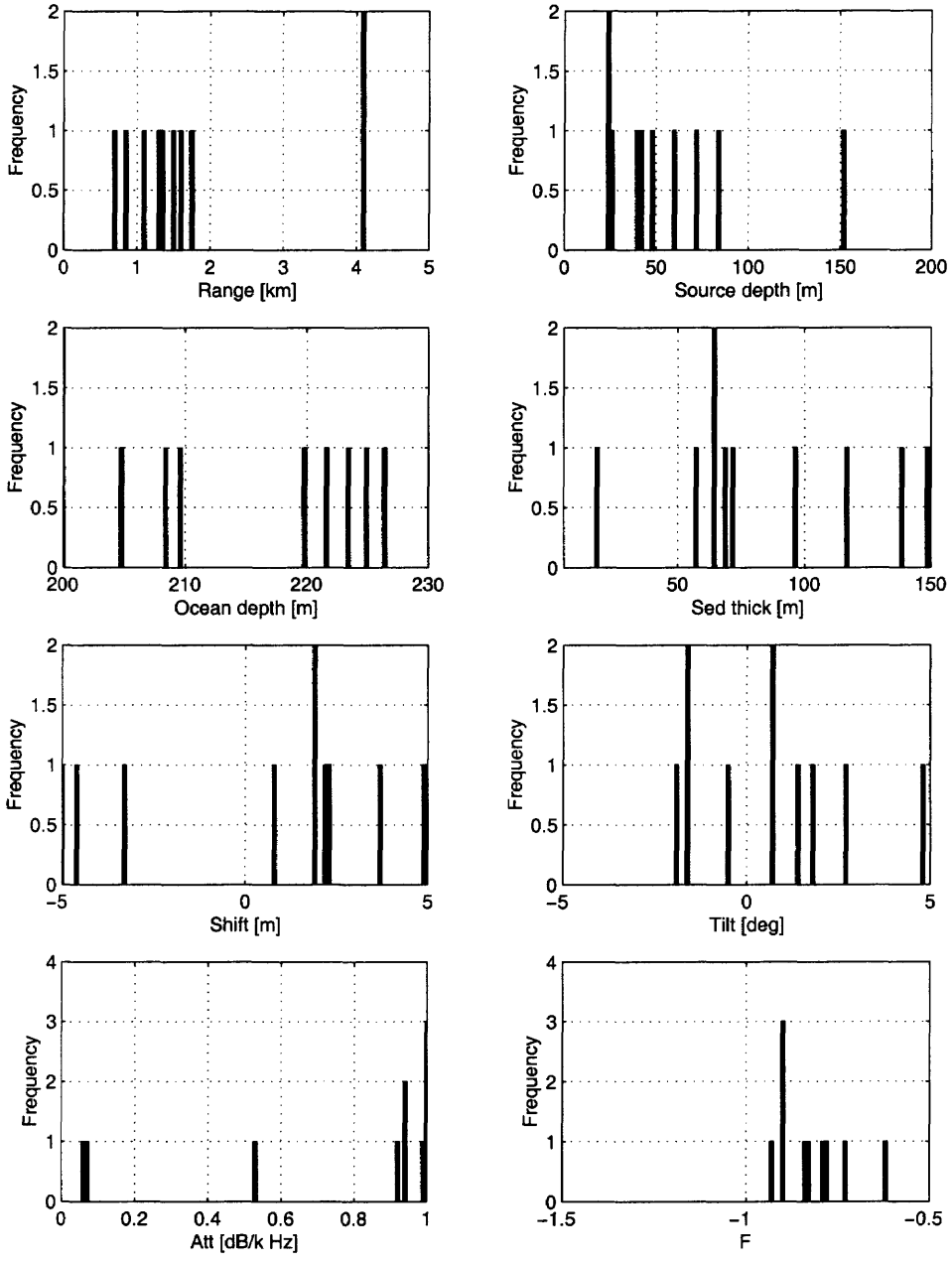

Figure 6.5 Histograms for real data seven-dimensional inversion.

Table 6.3 7D Real Data Inversion

r	1.3
sd	72.93
od	221.58
sed	18.66
shift	2.29
tilt	1.83
att	0.99
B	-0.62

is 1.83°. Taking tilt into account, a higher correlation is found at the new source location estimates.

Since inversion in a realistic environment is affected by several uncertainties, real data inversion often provides estimates of the parameters that differ from our prior knowledge. Considering such uncertainties, the estimates obtained from our inversion are quite promising.

Finally, we create a surface using source range and depth points explored by tabu for the seven-dimensional inversion (see Figure 6.6). Although we observe that there exists a side-lobe approximately at 1.6 km of range and 40 m of source depth, the main-lobe at 1.3 km of range and 73 m of source depth is very prominent.

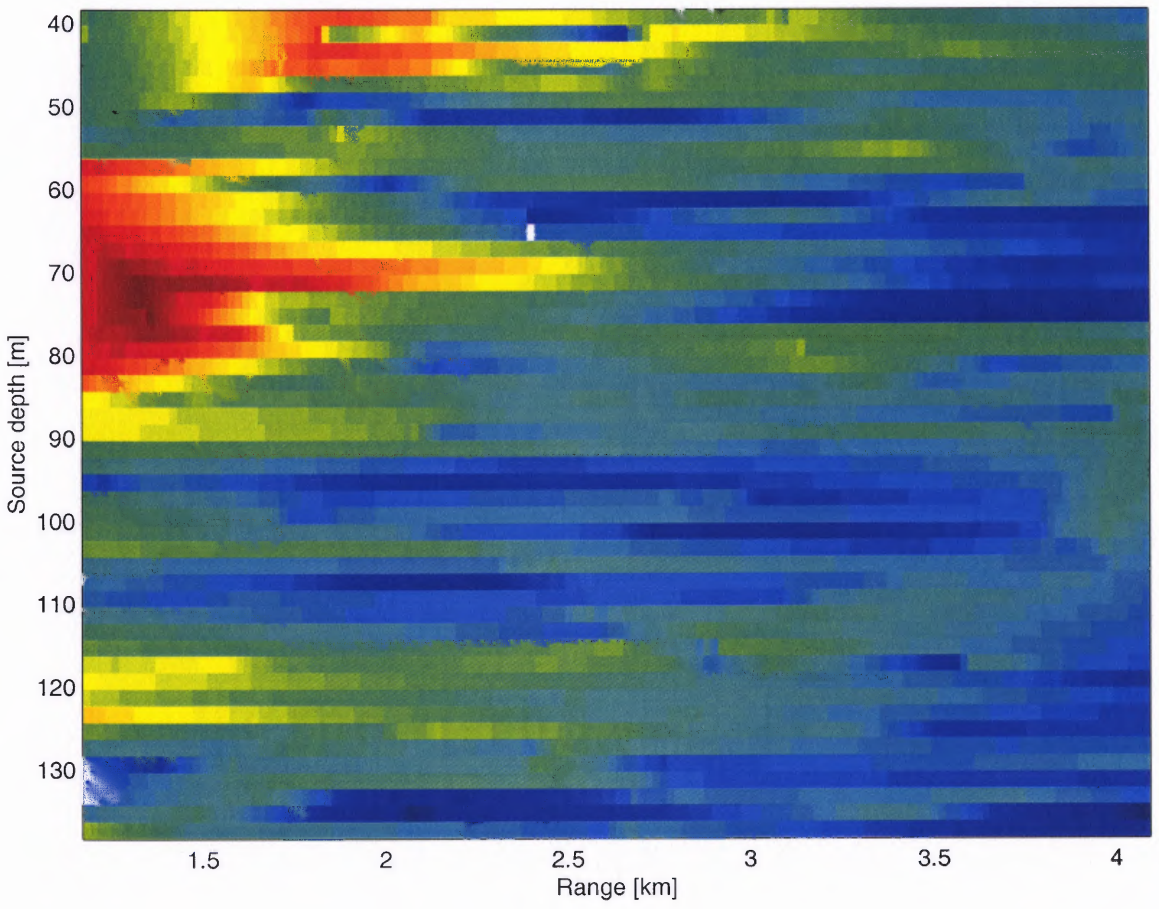

Figure 6.6 Surface obtained from source range and depth values visited by tabu in rotated coordinates for seven-dimensional real data inversion.

CHAPTER 7

CONCLUSIONS

Tabu is introduced as a global optimization technique in underwater acoustic signal processing. We develop three different lists based on three different criteria. Also, an escape mechanism is introduced here to avoid trapping. We have shown how this search learns from lists, prohibits moves and, thus, restricts the search space and continues moving from one search area to another by using random step jumps. Comparisons are provided between fast SA and tabu for three, six, seven, and nine-dimensional inversion. On average, tabu requires fewer forward model calculations than SA to reach higher maxima. Also, tabu finds, on average, better estimates of the unknown parameters than SA.

Next, coordinate rotation is discussed, and tabu is implemented in rotated coordinates. The results are, then, compared with the corresponding results obtained from tabu in conventional coordinates. We have shown that tabu in regular coordinates obtains always same or higher level of maxima than tabu in rotational axes. However, as dimensionality increases, tabu in rotated axes is more efficient than tabu in regular coordinates. Also SA in rotated coordinates is compared to the reparametrized tabu. We observe that tabu in rotated coordinates is more efficient than SA in rotated coordinates.

Finally, inversion is carried out with regular tabu and tabu in rotated coordinates with real data. The optimizing function used here is the geometric mean of Bartlett surfaces over all frequencies. For three-dimensional inversion, regular tabu and tabu in rotated coordinates locate the source efficiently and accurately. For the seven-dimensional inversion, the estimates are slightly different than expected. However, a higher maximum is obtained from the seven-dimensional inversion than from the three-dimensional exhaustive search.

Tabu could be improved by perturbing parameters preferentially. The more important parameters could be perturbed more frequently than the less important parameters. This approach might save many forward model calculations since the neighborhood size would be smaller.

BIBLIOGRAPHY

[1] Z.-H. Michalopoulou, "Matched-field processing for broad-band source localization," *IEEE Journal of Oceanic Engineering*, vol. 21, no. 4, pp. 384–385, 1996.

[2] H. P. Bucker, "Use of calculated sound fields and matched-field detection to locate sound sources in shallow water," *The Journal of the Acoustical Society of America*, vol. 59, no. 2, pp. 368–373, 1976.

[3] A. Tolstoy and O. Diachok, "Acoustic tomography via matched field processing," *The Journal of the Acoustical Society of America*, vol. 89, no. 3, pp. 1119–1127, 1991.

[4] A. B. Baggeroer, W. A. Kuperman, and P. N. Mikhalevsky, "An overview of matched field methods in ocean acoustics," *IEEE Journal of Oceanic Engineering*, vol. 18, no. 4, pp. 401–424, 1993.

[5] S. E. Dosso, M. L. Yeremy, J. M. Ozard, and N. R. Chapman, "Estimation of ocean-bottom properties by matched-field inversion of acoustic field data," *IEEE Journal of Oceanic Engineering*, vol. 18, no. 3, pp. 232–239, 1993.

[6] A. Tolstoy, *Matched Field Processing for Underwater Acoustics.* World Scientific, 1993.

[7] S. Kirkpatrick, C. D. Gelatt, and M. P. Vecchi, "Optimization by simulated annealing," *Science*, vol. 220, no. 4598, pp. 671–680, 1983.

[8] R. H. J. M. Otten and L. P. P. P. van Ginnekan, *The Annealing Algorithm.* Kluwer Academic Publishers, 1989.

[9] M. Sen and P. L. Stoffa, *Global Optimization Methods in Geophysical Inversion.* Elsevier Science B. V., 1995.

[10] W. A. Kuperman, M. D. Collins, J. S. Perkins, and N. R. Davis, "Optimal time-domain beamforming with simulated annealing including application of a priori information," *The Journal of the Acoustical Society of America*, vol. 88, no. 4, pp. 1802–1810, 1990.

[11] P. Gerstoft, "Inversion of seismoacoustic data using genetic algorithms and a posteriori probability distributions," *The Journal of the Acoustical Society of America*, vol. 95, no. 2, pp. 770–782, 1994.

[12] H. Szu and R. Hartley, "Fast simulated annealing," *Physics Letters A*, vol. 122, pp. 157–162, 1987.

[13] T. Kido, K. Takagi, and M. Nakanishi, "Analysis and comparisons of genetic algorithm, simulated annealing, tabu search, and evolutionary combination algorithm," *Informatica*, vol. 18, pp. 399–410, 1994.

[14] S. E. Dosso, "Quantifying uncertainty in geoacoustic inversion I.A fast Gibbs sampler approach," *The Journal of the Acoustical Society of America*, vol. 111, pp. 129–142, 2002.

[15] C. E. Lindsay and N. R. Chapman, "Matched field inversion for geoacoustic model parameters using adaptive simulated annealing," *IEEE Journal of Oceanic Engineering*, vol. 18, no. 3, pp. 224–231, 1993.

[16] N. R. Chapman and C. E. Lindsay, "Matched-field inversion for geoacoustic model parameters in shallow water," *IEEE Journal of Oceanic Engineering*, vol. 21, pp. 347–353, 1996.

[17] L. Jaschke, *Geophysical Inversion by the Freeze Bath Method with an Application to Geoacoustic Ocean Bottom Parameter Estimation.* Master's Thesis, University of Victoria, 1997.

[18] L. Jaschke and N. R. Chapman, "Matched field inversion of broadband data using the freeze bath method," *The Journal of the Acoustical Society of America*, vol. 106, pp. 1838–1851, 1999.

[19] M. R. Fallat and S. E. Dosso, "Geoacoustic inversion via local, global, and hybrid algorithms," *The Journal of the Acoustical Society of America*, vol. 105, pp. 3219–3230, 1999.

[20] F. Glover, "A user's guide to tabu search," *Annals of Operations Research*, vol. 41, pp. 3–27, 1993.

[21] F. Glover and M. Laguna, *Tabu Search.* Kluwer Academic Publishers, 1997.

[22] R. Vinther and K. Mosegaard, "Seismic inversion through Tabu Search," *European Association of Geoscientists and Engineers, Geophysical Prospecting*, vol. 44, pp. 555–570, 1996.

[23] D. Karaboga and D. T. Pham, *Intelligent Optimisation Techniques.* Springer Verlag, 2000.

[24] T. B. Neilsen, "Simultaneous source localization and environmental inversion using a rotated coordinates technique," *The Journal of the Acoustical Society of America*, vol. 89, no. 3, pp. 1119–1127, 2001.

[25] M. D. Collins and L. Fishman, "Efficient navigation of parameter landscapes," *The Journal of the Acoustical Society of America*, vol. 98, no. 3, pp. 1637–1644, 1995.

[26] F. Jensen, W. A. Kuperman, M. B. Porter, and H. Schmidt, *Computational Ocean Acoustics.* New York, New York: Springer-Verlag, 2000.

[27] M. B. Porter and E. L. Reiss, "A numerical method for ocean-acoustic normal modes," *The Journal of the Acoustical Society of America*, vol. 76, no. 1, pp. 244–252, 1984.

[28] M. B. Porter, "The KRAKEN normal mode program," *SACLANT Undersea Research Centre*, 1995.

[29] A. M. Richardson and L. W. Nolte, "A posteriori probability source localization in an uncertain sound speed, deep ocean environment," *The Journal of the Acoustical Society of America*, vol. 89, pp. 2280–2284, 1991.

[30] S. Geman and D. Geman, "Stochastic relaxation, Gibbs' distributions, and the Bayesian restoration of images," *IEEE Transactions on Pattern Analysis and Machine Intelligence*, vol. PAMI-6, pp. 721–741, 1984.

[31] M. D. Collins and W. A. Kuperman, "Focalization: environmental focusing and source localization," *The Journal of the Acoustical Society of America*, vol. 90, 1991.

[32] W. H. Press, A. Teukolsky, W. T. Vetterling, and B. P. Flannery, *Numerical recipes in FORTRAN: The Art of Scientific Computing.* Cambridge University Press, 1992.

[33] M. D. Collins, W. A. Kuperman, and H. Schmidt, "Nonlinear inversion for ocean-bottom properties," *The Journal of the Acoustical Society of America*, vol. 92, no. 5, pp. 2770–2783, 1992.

[34] Z.-H. Michalopoulou, "Matched-impulse-response processing for shallow-water localization and geoacoustic inversion," *The Journal of the Acoustical Society of America*, vol. 108, no. 5, pp. 2082–2090, 2000.

[35] N. O. Booth, A. T. Abawi, P. W. Schey, and W. S. Hodgkiss, "Detectibility of low-level broad-band signals using adaptive matched-field processing with vertical aperture arrays," *IEEE Journal of Oceanic Engineering*, vol. 25, no. 3, pp. 296–313, 2000.

[36] N. O. Booth, P. A. Baxley, J. A. Rice, P. W. Schey, W. S. Hodgkiss, G. L. D'Spain, and J. J. Murray, "Source localization with broad-band matched-field processing in shallow water," *IEEE Journal of Oceanic Engineering*, vol. 21, no. 4, pp. 402–412, 1996.

[37] R. T. Bachman, P. W. Schey, N. O. Booth, and F. J. Ryan, "Geoacoustic databases for matched-field processing: preliminary results in shallow water off San Diego, California," *The Journal of the Acoustical Society of America*, vol. 99, no. 4, pp. 2077–2085, 1996.

[38] A. B. Baggeroer, W. A. Kuperman, and H. Schmidt, "Matched field processing: source localization in correlated noise as an optimum parameter estimation problem," *The Journal of the Acoustical Society of America*, vol. 83, no. 2, pp. 571–587, 1988.